Molecular Therapy
Nucleic Acids
Original Article

Identification of selective and non-selective *C9ORF72* targeting *in vivo* active siRNAs

James W. Gilbert,[1] Zachary Kennedy,[1] Bruno M.D.C. Godinho,[1] Ashley Summers,[1] Alexandra Weiss,[2] Dimas Echeverria,[1] Brianna Bramato,[1] Nicholas McHugh,[1] David Cooper,[1] Ken Yamada,[1] Matthew Hassler,[1] Hélène Tran,[2] Fen Biao Gao,[1] Robert H. Brown, Jr.,[2] and Anastasia Khvorova[1]

[1]RNA Therapeutic Institute, Worcester, MA 01655, USA; [2]Department of Neurology, University of Massachusetts Chan Medical School, Worcester, MA 01655, USA

A hexanucleotide (G_4C_2) repeat expansion (HRE) within intron one of *C9ORF72* is the leading genetic cause of amyotrophic lateral sclerosis (ALS) and frontotemporal dementia (FTD). *C9ORF72* haploinsufficiency, formation of RNA foci, and production of dipeptide repeat (DPR) proteins have been proposed as mechanisms of disease. Here, we report the first example of disease-modifying siRNAs for *C9ORF72* driven ALS/FTD. Using a combination of reporter assay and primary cortical neurons derived from a C9-ALS/FTD mouse model, we screened a panel of more than 150 fully chemically stabilized siRNAs targeting different *C9ORF72* transcriptional variants. We demonstrate the lack of correlation between siRNA efficacy in reporter assay versus native environment; repeat-containing *C9ORF72* mRNA variants are found to preferentially localize to the nucleus, and thus *C9ORF72* mRNA accessibility and intracellular localization have a dominant impact on functional RNAi. Using a C9-ALS/FTD mouse model, we demonstrate that divalent siRNAs targeting *C9ORF72* mRNA variants specifically or non-selectively reduce the expression of *C9ORF72* mRNA and significantly reduce DPR proteins. Interestingly, siRNA silencing all *C9ORF72* mRNA transcripts was more effective in removing intranuclear mRNA aggregates than targeting only HRE-containing *C9ORF72* mRNA transcripts. Combined, these data support RNAi-based degradation of *C9ORF72* as a potential therapeutic paradigm.

INTRODUCTION

Amyotrophic lateral sclerosis (ALS) and frontotemporal dementias (FTDs) are recognized as two ends of a clinical continuum of disease. ALS is characterized by the degeneration of upper and lower motor neurons, leading to progressive paralysis and ultimately death, whereas FTD is characterized by focal degeneration in the prefrontal and/or temporal lobes, resulting in changes in personality, language, social behaviors, and other abnormalities. Clinical observations show that 50% of patients diagnosed with ALS also display FTD-associated cognitive impairment,[1] and 37% of FTD cases display motor dysfunction.[2] Globally, approximately 40,000 people die of ALS each year, with an incidence of 18,000 new diagnoses each year.[3] Despite the growing interest in this disease, there is still a large unmet medical need. Currently, only three therapeutics for ALS have received US Food and Drug Administration approval—riluzole, edaravone, and relyvrio which has since been removed from the market. None of these therapeutics are disease modifying, and they provide only limited benefit.[4–6]

A hexanucleotide repeat expansion (HRE) of GGGGCC (G_4C_2) within intron one of chromosome 9 open reading frame 72 (*C9ORF72*)[7,8] is the leading genetic cause of ALS and FTD, accounting for 35% of all ALS cases (57% of familial, 14% of sporadic) as well as 6% of all FTD cases (9% of familial, 4% of sporadic).[9] It is estimated that ∼4,500 people live with *C9ORF72*-driven ALS (C9-ALS),[10] with an earlier age of disease onset and a shorter survival time than ALS patients without the HRE. Specifically, C9-ALS patients have a younger age at disease onset of 56.3 versus 61.3 years, with a survival of 20 months vs. 26 months without *C9ORF72* expansion.[11]

The *C9ORF72* gene contains two alternative promoters, three alternative first exons, and two alternative last exons producing three transcript variants: V1, V2, and V3 (Figure 1A). Across diverse cell lineages, V2 is the primary transcript variant, representing 92.6% ± 1.2% of all *C9ORF72* transcripts,[12] and along with V3, produces the C9ORF72 protein, which regulates autophagosomal and lysosomal biogenesis and function, inflammation, and trafficking.[13–18] V1 and V3 share a common promotor, and pre-mRNA, which contains the HRE, have alternative exon 1 3′ splice sites.

While the exact mechanism of *C9ORF72*-mediated neurodegeneration is still unclear, three non-mutually exclusive pathogenic mechanisms have been proposed. The G_4C_2 expansion, due to its localization 5′ to the promoter of V2, is proposed to be involved in hypermethylation leading to reduced expression of the C9ORF72 protein, and therefore the implied loss of function called haploinsufficiency.[19–21] Genetic knockout of the mouse ortholog of *C9ORF72* (3110043O21Rik) specifically in neuronal cells does not induce motor neuron degeneration,[22] and whole-mouse ablation does not affect motor function. Interestingly, *C9ORF72*-null mice develop

Received 3 January 2024; accepted 29 July 2024;
https://doi.org/10.1016/j.omtn.2024.102291.

Correspondence: Anastasia Khvorova, RNA Therapeutic Institute, Worcester, MA 01655, USA.
E-mail: anastasia.khvorova@umassmed.edu

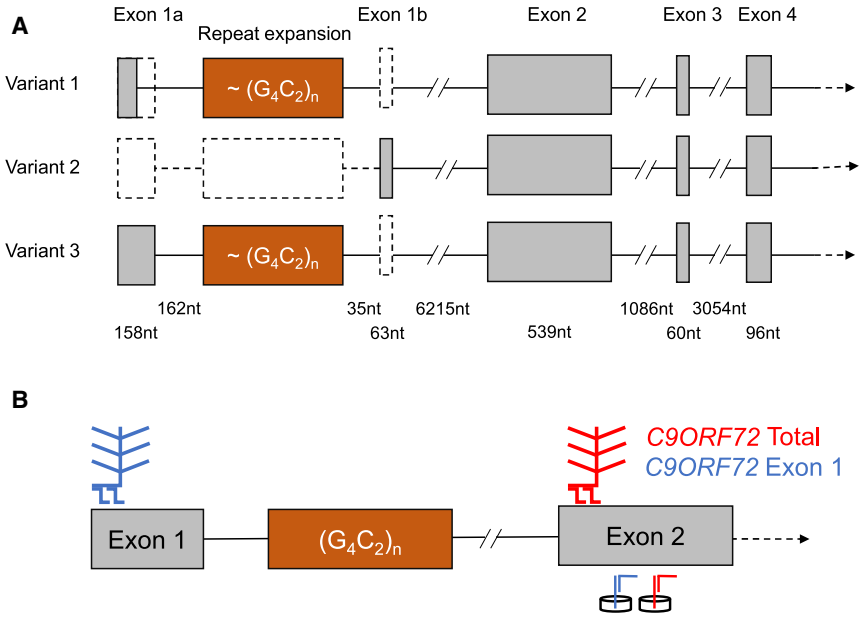

Figure 1. *C9ORF72* mRNA transcriptional variants are differentially expressed throughout the mouse CNS

(A) Schematic of differential processing of repeat-containing and non-repeat-containing *C9ORF72* mRNA variants. (B) C57BL/6J-Tg(C9orf72_i3) mice harboring the human C9ORF72 transgene were assessed for C9ORF72 mRNA throughout the CNS. QuantiGene probes were designed to specifically identify mRNA variants containing the G4C2 expansion, or non-selectively identify all C9ORF72 mRNA variants. (C) Relative level of expression of repeat-containing and total *C9ORF72* mRNA in primary cells and mouse tissues. Error bars represent biological variation. n = 3-7.

non-CNS complications that are not associated with ALS, including splenomegaly and infiltration of macrophages into multiple organs such as liver, kidney, and lung.[13,23]

Toxic RNA caused by aberrant bilateral transcription of the HRE has been proposed to cause toxicity through an RNA-mediated dynamic sequestration of RNA-binding proteins such as hnRNP H1/F and ALYREF[24] or disruption of nucleocytoplasmic transport.[25] The HRE can itself be trafficked into the cytoplasm through inappropriate association with mRNA export adaptor proteins,[24] leading to the formation of toxic dipeptide repeat (DPR) proteins.[26] DPR proteins have been shown to exert toxicity through the disruption of protein synthesis, mitochondrial damage, impairing nucleocytoplasmic transport and other cellular processes.[27–31]

Given that evidence of all three mechanisms cause some form of dysregulation, it is possible that all three contribute to toxicity. Indeed, synergistic mechanisms between haploinsufficiency, RNA toxicity, and DPR toxicity has been proposed recently.[32,33]

Different classes of therapeutic oligonucleotides have been developed for genetically defined diseases, including antisense oligonucleotides (ASOs) and small interfering RNAs (siRNA). ASOs were one of the first developed and act through RNase H-mediated mRNA cleavage or non-cleaving steric blockage mechanisms. siRNA are small double-stranded oligonucleotides, where one of the strands loads into a protein complex, RNA-induced silencing complex (RISC), and guides endogenous RNAi enzymatic activity to cleave target mRNAs.[34] Both approaches allow the modulation of disease-linked mRNAs, blocking progression of genetically defined disorders.

Several ASOs have been developed to selectively silence *C9ORF72* mRNA. They demonstrate great potential to reduce *C9ORF72* mRNA and DPR proteins in preclinical models.[35–38] Selective silencing of repeat-containing isoforms in clinical trials by ASOs has resulted in potent reduction of DPR proteins.[39,40] Unfortunately, this reduction in DPR proteins has not translated into a therapeutic benefit. In one clinical trial, C9-ALS patients treated with an ASO showed no benefit, with worsening of clinical score and a significant increase in neurofilament light,[41] a common biomarker of general neurodegeneration. While the interpretation of the clinical data is ongoing, it highlights the requirement to develop novel strategies.

Many groups have identified functional ASOs against *C9ORF72*; however, developing the ability to identify effective siRNAs has been unsuccessful.[35–37,40,41] One study was able to identify siRNAs that reduce *C9ORF72* by 70% in patient induced pluripotent stem

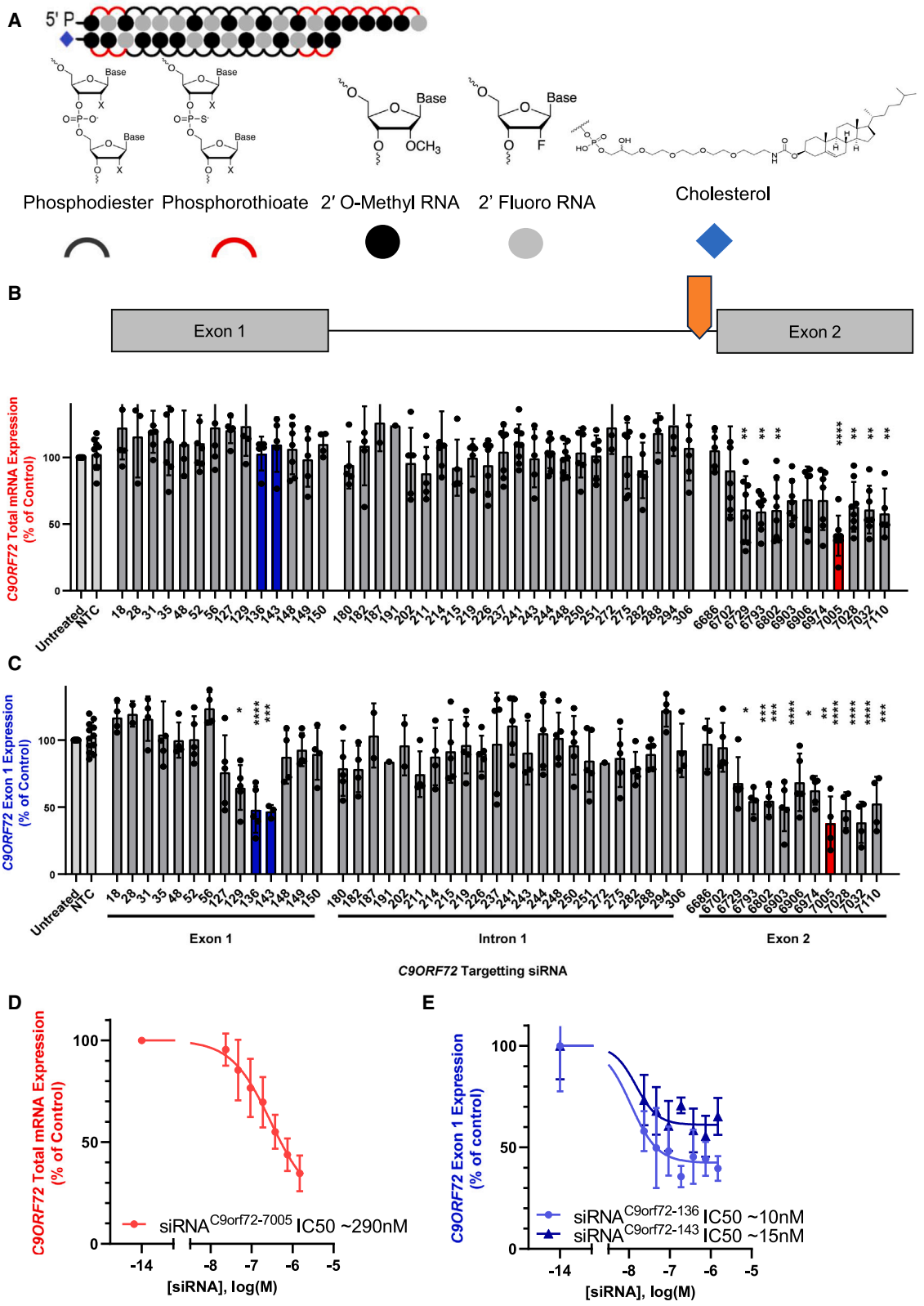

(legend on next page)

cell-derived neurons. RNA foci were unaffected, however.[36] This discrepancy was explained by the assumed preferential activity of siRNAs in the cytoplasm, while RNA foci are found in the nucleus and therefore unavailable to RNAi-mediated reduction.

We have recently identified a novel siRNA scaffold that enables widespread distribution in the brains of rodents and sheep and efficiently reduces the expression of target genes in the CNS of rodents and non-human primates (NHPs) for 6 months after a single injection.[42,43]

Here, we report extensive screening of a panel of fully chemically stabilized siRNAs that efficiently silence *C9ORF72* mRNA variants in primary neurons and *in vivo*. siRNAs designed to target exon 1 selectively reduce HRE-containing transcripts while sparing transcript variant 2. Additionally, siRNAs were designed to target exon 2 or exon 4 to reduce all *C9ORF72* transcript variants. The vast majority of reporter-active siRNAs targeting *C9ORF72* variants failed to silence the target in a native context. Preferential nuclear localization and clustering of mutant *C9ORF72* mRNA is likely limiting accessibility of the transcript to the RNAi machinery. *In vitro* and *in vivo* experiments in a preclinical mouse model of C9-ALS/FTD presented here demonstrate the reduction of *C9ORF72* repeat-containing transcripts and/or all *C9ORF72* mRNA transcripts in addition to reducing C9-ALS/FTD markers of disease, RNA foci and DPR proteins.

RESULTS

Screening and identification of fully chemically stabilized siRNAs selectively and non-selectively targeting *C9ORF72* mRNA transcriptional variants

A panel of siRNAs was designed to target either all *C9ORF72* mRNA isoforms or only mRNA isoforms containing the HRE (Figure 1A). The sequences and chemical modification patterns of all compounds used in the study are shown in Tables S1 and S2. To detect *C9ORF72* expression, branched DNA probes (Quantigene 2.0) were designed to detect HRE-containing *C9ORF72* mRNA via binding to exon 1 or all *C9ORF72* mRNAs via binding to exon 2 (Figure 1B). The relative abundance of exon 1-containing transcripts compared to total *C9ORF72* mRNA was measured across multiple neuronal cell types and tissues from an ALS/FTD mouse model (Figure 1C). Consistent with previously published data demonstrating HRE-containing RNA composes a small portion of total *C9ORF72* RNA,[44] the relative expression of exon 1-containing *C9ORF72* mRNA was around 10% of total *C9ORF72* expression in all cell types and tissues assessed. As such, it is expected that siRNA designed to target exon 1 or intron 1 (i.e., HRE-containing *C9ORF72* mRNA) will have little effect on overall *C9ORF72* mRNA levels.

We designed a panel of 48 siRNAs using an algorithm that filtered and scored all possible *C9ORF72* target sequences using previously published criteria.[45] The top 36 sequences targeting either exon 1 or intron 1, and the top 12 sequences targeting exon 2 were synthesized onto a fully chemically stabilized scaffold (Figure 2A). siRNAs were tested in primary cortical mouse neurons derived from an established ALS/FTD mouse model (C9-BAC [C57BL/6J-Tg(C9orf72_i3)112Lutzy/J]),[46] and *C9ORF72* mRNA levels were quantified 72 h later using the QuantiGene assay (Figure 1B).

Of the 37 siRNAs designed to target exon 1 or intron 1, none showed significant reduction of total *C9ORF72* mRNA (Figure 2B), an expected result given that exon 1-containing *C9ORF72* composes 10% of total *C9ORF72*. When assessing the expression of exon 1-containing RNA, however, two siRNAs targeting exon 1 achieved a 50% reduction (Figure 2C).

For exon 2-targeting siRNAs, 7 out of 12 significantly reduced both total *C9ORF72* mRNA and exon 1-containing *C9ORF72* mRNA (Figures 2B and 2C, respectively).

Three lead siRNAs were further examined using concentration response curves to determine relative siRNA potency. The top-performing siRNA targeting exon 2 is shown in Figure 2D, and the other lead siRNAs targeting exon2 are shown in Figures S1A–S1D and Table S3. The top-performing siRNAs targeting exon 1 are shown in Figure 2E.

Interestingly, the functional hit rate (i.e., the number of active siRNAs in the panel) was much lower than anticipated for this class of compounds (data not shown). Only 2 out of 14 siRNAs targeting *C9ORF72* exon 1 and 0 out of 23 siRNAs targeting *C9ORF72* intron 1 showed significant efficacy. While the hit rate is highly affected by the target, it usually ranges between 5% and 60%.[47–49] The unusually low siRNA hit rate suggests that factors other than efficient RISC interactions may be limiting the efficacy of *C9ORF72* targeting via siRNAs.

C9ORF72 targeting siRNA efficacy from a reporter system does not correlate with silencing efficacy in primary neurons

To confirm that our chemically modified siRNAs targeting *C9ORF72* were able to load into Ago2 and form an active RISC capable of reducing target RNA, we evaluated efficacy of the siRNA panel in a luciferase reporter assay. A reporter construct was generated by cloning siRNA-targeted regions into the 3′ UTR of the *Renilla* luciferase of the psiCHECK2 plasmid[50–54] (Table S5). This plasmid contains

Figure 2. Screening and identification of fully chemically stabilized siRNAs selectively and non-selectively targeting *C9ORF72* mRNA transcriptional variants

(A) Chemical configuration of siRNAs used for screening. (B and C) Primary neurons derived from C57BL/6J-Tg(C9orf72_i3) mice were treated with 1.5 μM *C9ORF72* targeting siRNAs (exon 1, intron 1, and exon 2) and levels of full-length C9ORF72 mRNA (B) and exon 1-containing C9ORF72 transcripts (C) were evaluated at 1 week by QuantiGene (n = 3–9, mean ± SD, one-way ANOVA, Dunnett's multiple comparison correction; $^{*}p < 0.05$; $^{**}p < 0.01$; $^{***}p < 0.001$; $^{****}p < 0.0001$). (D and E) Lead compounds show concentration-dependent reduction of C9ORF72 total (D) and exon 1-containing (E) variants.

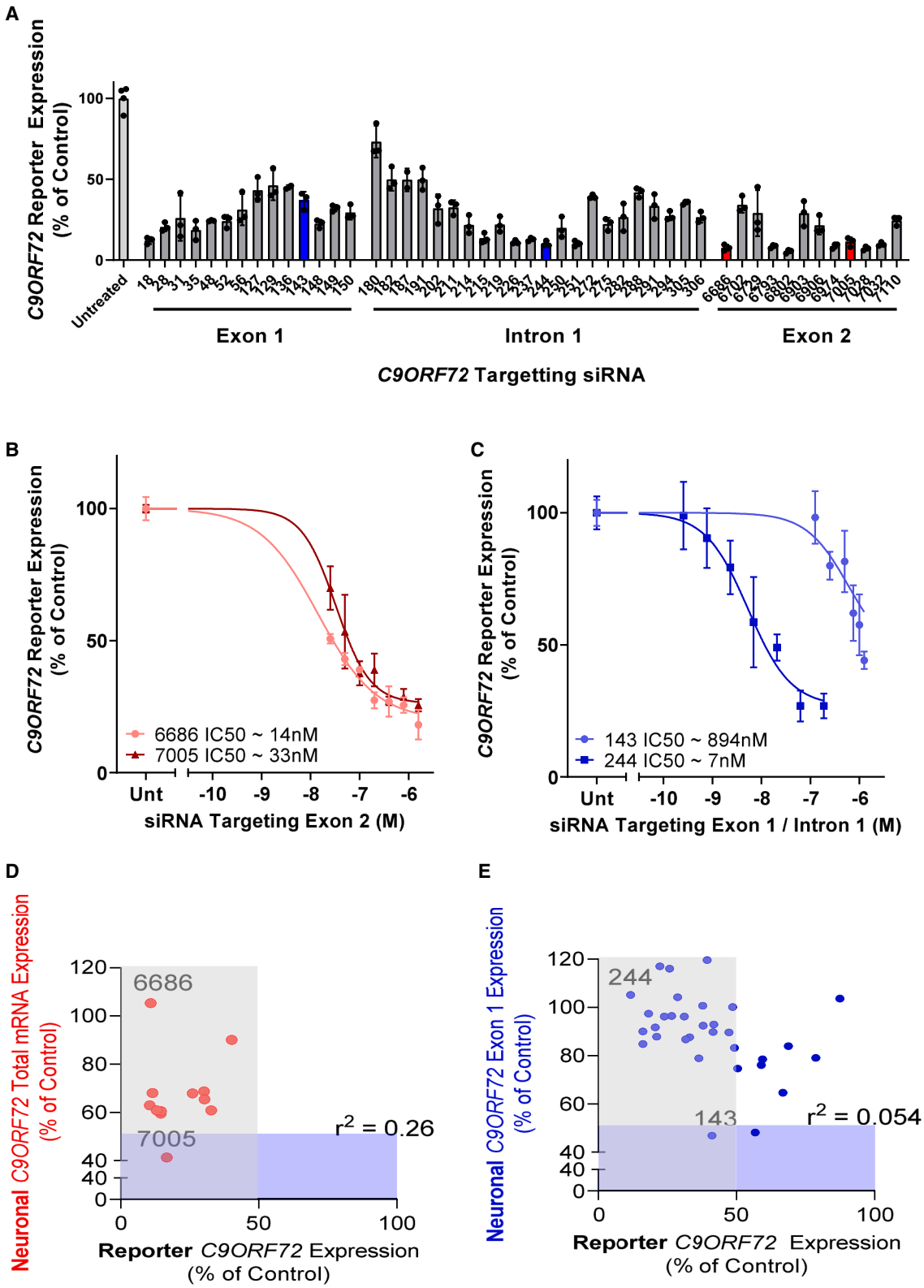

(legend on next page)

Renilla luciferase and an independently transcribed firefly luciferase reporter gene, which can account for variation in transfection efficiency and cell viability. Efficacy of siRNA in this system was defined as a reduction in luminescence from *Renilla* luciferase.

In stark contrast to the screen in primary mouse cortical cells in which only 2 out of 14 siRNAs targeting exon 1 or intron 1 were active, every single siRNA targeting exon 1 and intron 1 (36 total) displayed efficacy, with knockdown percentages ranging from 25% to 90% (Figure 3A; Table S6). Furthermore, 8 out of 36 siRNAs achieved greater than 80% reduction. These findings suggest that our chemically modified siRNAs are capable of loading into Ago2 and producing active RISCs.

Interestingly, the results from the screen in the reporter system did not correlate well with results from the screen in the primary neurons. For siRNAs targeting HRE-containing *C9ORF72* (e.g., siRNAs targeting exon 1 or intron 1), previously identified lead siRNA 143 from the neuronal screen did not produce the greatest reduction in the luciferase-based assay (Figure 2C). Four siRNAs that targeted a region within intron 1 of *C9ORF72* between nucleotides 226 and 251, outperformed previously identified lead compound 143 with half-maximal inhibitory concentration (IC_{50}) values 100 times lower than the previously identified lead (Figure S4). The results for the exon 2 screen were more consistent between the primary neuron and the *Renilla* reporter screen, with previous leads from the neuronal screen appearing among the most efficacious in the reporter assay. Figure 3D visualizes the relative efficacy of siRNA in these two screens. There is no correlation between either exon 1- or intron 1-targeting compounds, suggesting that factors other than RISC entry limits efficacy. The differences in the exon 2 targeting panel were less pronounced, with at least one of the previous leads (siRNA 7005) showing efficacy in both systems. Screening in the reporter assay confirmed that a large fraction of siRNAs designed to target *C9ORF72* mRNA is highly efficient in RISC entry and target sequence cleavage in a context of the reporter. This indicates that factors other than RISC function limit the ability of siRNA to target *C9ORF72* mRNA variants in the native context. These may be mRNA secondary structure, RNA-binding proteins, RNA aggregation, or intracellular localization. This emphasizes the importance of using "native" context when identifying compounds to target potentially structured RNA variants. At this stage, sequences that showed efficacy in both screening approaches were chosen as leads.

C9ORF72 repeat-containing and non-repeat-containing isoforms form nuclear clusters in astrocytes derived from C9-ALS/FTD mice

The highly divergent results generated from a reporter and native mRNA context indicate that factors specific to *C9ORF72* mRNA intracellular localization are primarily limiting siRNA efficacy. The screen was repeated in a non-neuronal cell type (astrocytes) (Figures S2 and S3; Table S4) and this confirmed the data observed in Figure 2. To evaluate intracellular localization of the *C9ORF72*, astrocytes derived from C9-ALS/FTD mice were used to evaluate *C9ORF72* mRNA variants localization using an advanced RNA *in situ* hybridization technique (RNAscope) that permits visualization of single RNA species with high sensitivity and low background. The RNAscope probes were designed to detect intron 1 (specific to repeat-containing isoforms), all human *C9ORF72* isoforms, mouse *C9orf72*, and housekeeping gene *Hprt* (hypoxanthine-guanine phosphoribosyltransferase).

In wild-type astrocytes, the mouse *C9orf72* mRNA shows unremarkable distribution, with the majority of individual foci localized cytoplasmically (Figure S7). In astrocytes derived from C9-ALS/FTD mice, the mouse *C9orf72* distribution is not perturbed, while the human transgene shows remarkably different localization patterns. Human mutant *C9ORF72* is preferentially located to the nuclei and shows a tendency toward aggregate in large intranuclear clusters (Figure S7).

When cells were simultaneously stained with both intron 1 (repeat selective) and a pan-isoform *C9ORF72* probe, a significant colocalization was observed. Approximately 80% of clusters were positive for the intron 1-containing variants. The observed co-localization was specific and non-random, as rotation of the image in one of the channels resulted in an almost complete loss of overlap.

The observed intranuclear aggregation of mutant human *C9ORF72* explains the low hit rate and relatively lower IC_{50} values for the identified siRNAs hits. It is likely that accessibility to the cluster or intranuclear mRNA is significantly limiting observed RNAi-based reduction of *C9ORF72* expression.

C9ORF72 targeting siRNA injected into a C9-ALS mouse model displays robust mRNA reduction

To investigate the ability of siRNA to reduce *C9ORF72* transcripts *in vivo*, we transferred the sequence onto a chemical scaffold that demonstrates distribution and efficacy throughout the mouse brain after a single intracerebroventricular (ICV) injection[42] (Figure 4A). This configuration utilizes the divalent scaffold, which slows cerebrospinal fluid (CSF) clearance and enhances neuronal uptake.[42,43] In addition, the incorporation of the 5′ vinyl phosphonate as the guide modification enhances RISC affinity, provides phosphatase resistance, and enhances *in vivo* efficacy.[55,56] Ninety-day old C9-ALS/FTD mice were dosed using a bilateral ICV injection containing 10 nmol (∼240 μg, ∼120 μg per ventricle) total siRNA targeted against either *C9ORF72*

Figure 3. The *C9ORF72* targeting siRNA efficacy from a luciferase-based reporter does not correlate with silencing efficacy in primary neurons

(A) *C9ORF72* targeting siRNAs efficacy were evaluated in a dual-luciferase reporter (psiCHECK2) system, in which targeting regions were cloned in the 3′ UTR of *Renilla* luciferase. Activity of siRNAs was calculated as a reduction in firefly luciferase, normalized against the *Renilla* transfection control. HeLa cells were treated with 1.5 μM *C9ORF72* targeting siRNAs for 72 h ($n = 3$, mean ± SD). (B and C) Lead compounds show concentration-dependent reduction of C9ORF72 total (B) and exon 1-containing (C) variants. (D and E) The relative efficacy of *C9ORF72* in reporter and primary neurons.

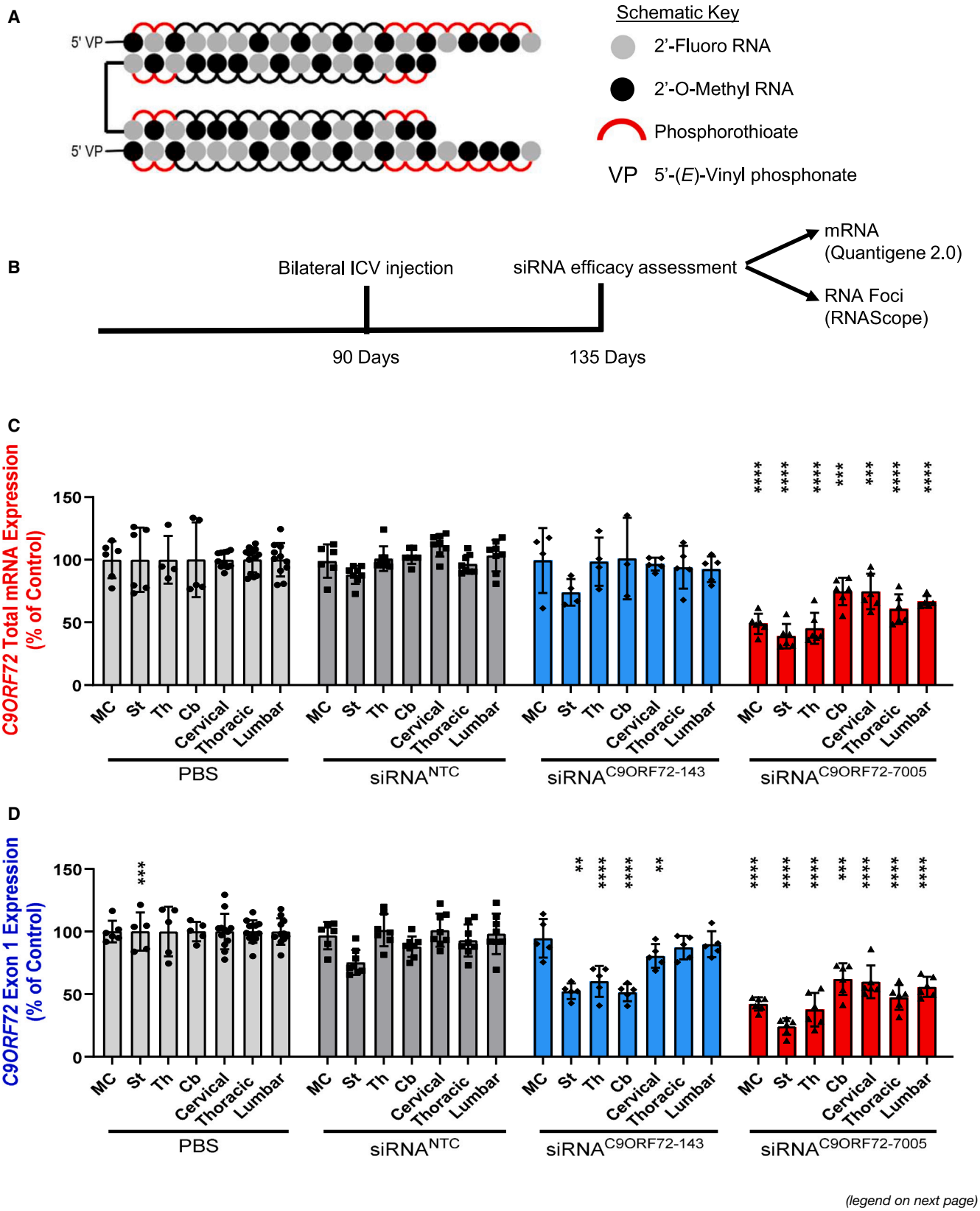

(legend on next page)

exon 1 (divalent [di]-siRNA 143), *C9ORF72* exon 2 (di-siRNA 7005), or dosed with a non-targeting control (NTC) or with PBS. Six weeks post injection, mice were assessed for siRNA efficacy. siRNA targeting exon 1 display no reduction in total *C9ORF72* mRNA, except for a modest reduction observed in the striatum, a region proximal to the site of injection (Figure 4C). Mice treated with siRNA targeting *C9ORF72* exon 2 mRNA display 25%–60% reduction of total *C9ORF72* mRNA throughout the brain, with greater reduction seen in tissues proximal to the site of administration, as well as 25%–40% mRNA reduction in the spinal cord (Figure 4C). siRNA targeting *C9ORF72* exon 1 display 40%–50% reduction of transcript V1/V3 around the site of injection and posteriorly in the cerebellum, but interestingly, only 20% anteriorly in the motor cortex, as well as 20% reduction in the spinal cord. siRNA targeting *C9ORF72* exon 2 mRNA display 65%–75% reduction of transcript V1/V3 close to the site of injection, and 40%–60% reduction distally and throughout the spine (Figure 4D). These results are consistent with the specific and non-specific targeting strategies outlined in Figures 1A and 1B and with our *in vitro* screening results (Figures 2B and 2C). Investigation of the clearance organs, such as liver and kidney, reveals that siRNA administered into the brain through an ICV injection have no impact on *C9ORF72* total mRNA levels or a minimal impact on *C9ORF72* V1/V3 RNA levels (Figure S5).

Targeted siRNA screen around position 136 of *C9ORF72* exon 1 identifies region highly accessible to RNAi machinery

To further optimize siRNAs specific for repeat-containing variants, we utilized primary neurons from C9-ALS/FTD mice to perform a single nucleotide walk across the exon 1 of *C9ORF72* (Figure 5A; Table S7). All siRNAs targeting exon 1 displayed no total *C9ORF72* mRNA reduction (Figure 5B). The two previously identified sequences (136 and 143) appear to be the edges of a productive region, with target sequences flanking this region appearing inactive. Across the productive region, 136–143, siRNAs display 50%–70% V1/V3 mRNA reduction (Figure 5D), similar to levels observed previously. siRNA targeting within this region was further investigated using concentration response curves, with one of the originally identified sequences among the most potent (Figures 5D–5G and S6; Table S8). Secondary mRNA structures are known to have a large impact on siRNA efficacy, and we hypothesize that this region is more productive for siRNA reduction due to a favorable local mRNA environment. These data confirm that siRNAs targeting positions 136, 140, and 143 are the most efficacious and potent V1/V3 variants specific siRNA compounds.

Broad siRNA screens across exons 2,4,5 of *C9ORF72* identify additional non-selective functional siRNAs

Additionally, we expanded the screen for non-selective siRNAs targeting all *C9ORF72* mRNA variants. Primary neurons derived from the C9-ALS/FTD mice were treated with siRNAs targeting *C9ORF72* exons 2,4,5 (Figure 6A; Table S9). Five additional compounds (two in exon 2, two in exon 4, and one in exon 5) showed efficacy similar or greater compared to our previously identified lead siRNA, siRNA 7005 (Figure 6B). To define the relative potency, identified siRNAs efficacy was compared in a wide dose range (Figures 6C–6E). In this experiment, the relative potency of the previously identified siRNA 7005 was lower, which is likely due to a different chemical scaffold used. Within the experiment, the siRNA targeting the end of the exon 4 (siRNA 11437) was ∼4-fold more potent than siRNA 7005 (siRNA 7005, IC_{50} ∼1,200 nM vs. siRNA 11437, 450 nM).

C9ORF72 targeting siRNA injected into a C9-ALS/FTD mouse model display robust RNA and DPR reduction

The new lead siRNA compounds specific for the repeat-containing (di-siRNA 136) (Figure 5D) and all *C9ORF72* mRNA transcripts (di-siRNA 11437) (Figure 6B) were synthesized in the divalent CNS-active scaffold (Figure 7A), injected into C9-ALS/FTD mice at 90 days old and assessed for mRNA and DPR reduction 4 weeks later.

siRNA targeting V1/V3 show no impact on *C9ORF72* total mRNA levels across the brain or spinal cord, whereas di-siRNA 11437 (exon 4) show up to 40% reduction in total *C9ORF72* mRNA in the brain as well as in the spinal cord (Figure 7C).

siRNA targeting exon 1 selectively reduces *C9ORF72* V1/V3 RNA by 10%–30% throughout the brain, whereas non-selective exon 4 targeting siRNA reduces V1/V3 RNA by 50% in regions close to the site of injection (Figure 7D). In the spine, siRNA targeting exon 1 selectively reduces V1/V3 RNA by 40%, and non-selective exon 4 targeting siRNA reduces V1/V3RNA by 50% (Figure 7D).

Mice from this study were further evaluated for DPR protein reduction, a key marker of C9-ALS/FTD, using an ELISA measuring poly(GP). siRNA targeting exon 1 were able to reduce poly(GP) by ∼60% in the motor cortex, which is a disease-relevant region. Consistent with mRNA findings, the exon 4 targeting siRNA reduced poly(GP) to a greater degree, with a reduction of 50%–65% across the brain (Figure 7E). siRNA targeting exon 4 was also more efficacious in reducing poly(GP) throughout the spine, with 75%–85% reduction observed, compared to 30%–60% reduction for siRNA targeting exon 1 (Figure 7E).

The level of observed silencing varied between different brain/spinal cord regions, but overall, non-selective siRNA was much more potent in silencing repeat-containing isoforms on both mRNA and peptide levels.

Figure 4. *C9ORF72* targeting siRNAs injected into a C9-ALS mouse model display robust mRNA reduction

(A) Divalent siRNA scaffold used for *in vivo* studies. (B) C57BL/6J-Tg(C9orf72_i3) mice were treated via bilateral ICV injection with 10 nmol (240 μg) siRNAs targeting C9ORF72-143 (exon 1), C9ORF72-7005 (exon 2), NTC, and PBS. Levels of *C9ORF72* variant (C, total; D, exon 1) expression were evaluated at 6 weeks post-injection (n = 3–13, mean ± SD; two-way ANOVA, Dunnett's multiple comparison correction; $^{**}p < 0.01$; $^{***}p < 0.001$; $^{****}p < 0.0001$).

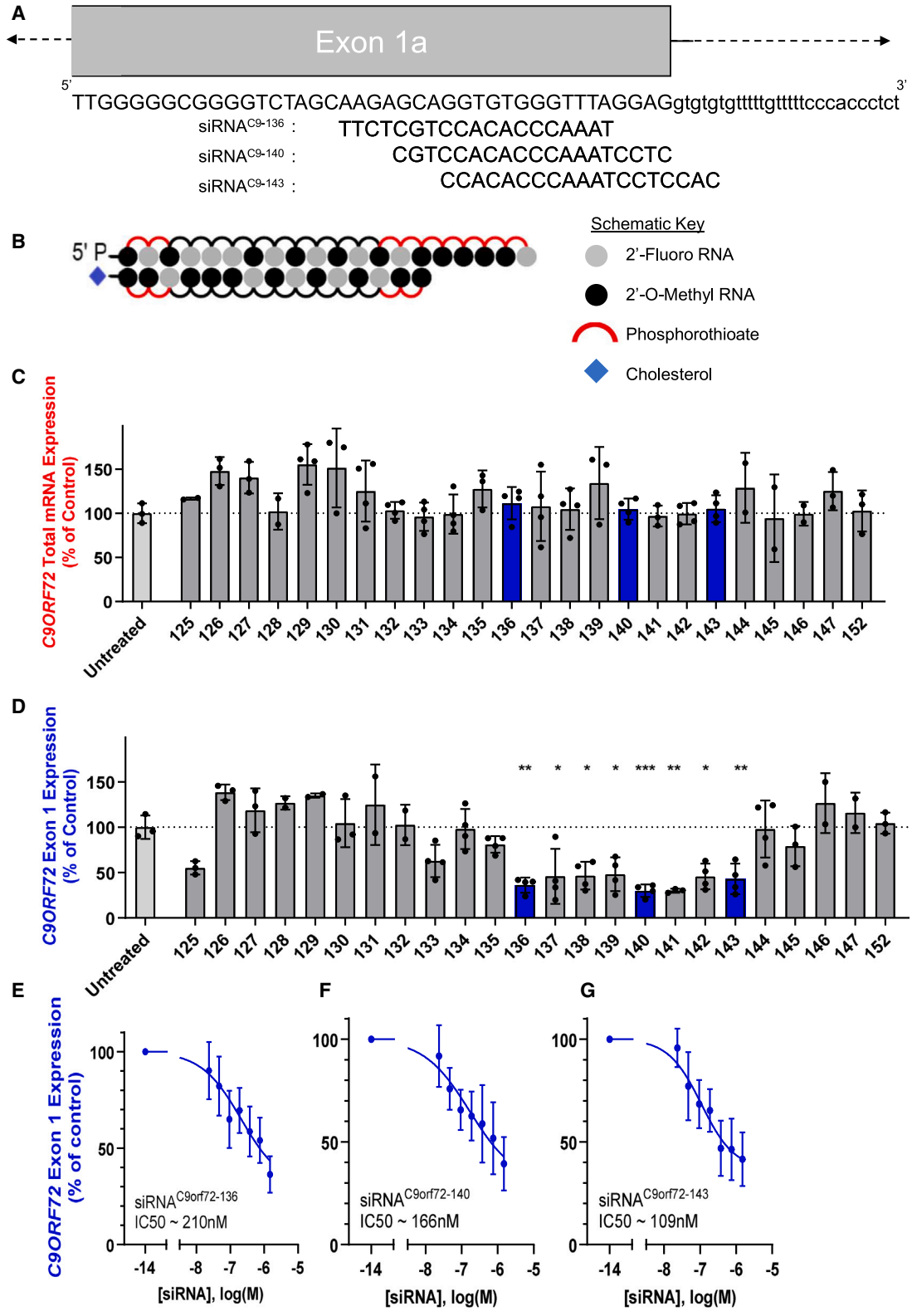

(legend on next page)

C9ORF72-targeting siRNA reduces RNA but not intranuclear RNA aggregates

Intranuclear RNA aggregates are a hallmark of *C9ORF72*-driven ALS. To assess whether C9-ALS/FTD mice injected with di-siRNA 136 (exon 1) and di-siRNA 11437 (exon 4) displayed a reduction in RNA aggregates, we further evaluated these mice using RNAscope. Brain sections from mice treated with di-siRNA 136 (exon 1), di-siRNA 11437 (exon 4), and NTC were stained with pan-isoform *C9ORF72* probes and visualized using confocal microscopy. Stereotactically cut slices from three mice were used for the visualization, and data from 170 to 220 randomly selected cells were quantified.

Total *C9ORF72* mRNA shows extreme variability in expression levels, with some cells having dozens of foci, localized equally between nuclei and cytoplasm, and others showing no detectable expression (Figure 8A). Additionally, similar to astrocytes, we observe mutant *C9ORF72* mRNA forming large intranuclear clusters in approximately half of the assumed neuronal cells (Figures 8A and S7).

Treatment with selective di-siRNA 136 shows no impact on *C9ORF72* mRNA nuclear foci and some reduction in the number of the cytoplasmic foci. While there is no change in the total *C9ORF72* expression (Figure 7C), the observed reduction in cytoplasmic foci (Figure 8C) indicates that silencing of the repeat-containing isoforms might alter the intracellular distribution of the major *C9ORF72* isoform. Treatment with non-selective di-siRNA 11437 resulted in a statistically significant reduction of both cytoplasmic and nuclear C*9ORF72* mRNA foci and profound changes in the observed distribution (Figures 8B and 8C).

Quantification of the RNAscope staining (see materials and methods) reveals that the *C9ORF72* exon 2 mRNA is distributed between nuclei and cytoplasm, with a slight preference for cytoplasmic localization. After treatment with di-siRNA 136, the slight shift toward nuclear localization is observed as likely due to a reduction in the number of the cytoplasmic foci (Figure 8B). Treatment with pan-isoform targeting di-siRNA 11437 resulted in a further shift toward nuclear localization, likely due to the preferential silencing of the cytoplasmic mRNAs (Figure 8B). This suggests that for both siRNA treatments, the mRNA residing in the cytoplasmic compartment is preferentially degraded.

Further analysis reveals that di-siRNA 136 has a minor impact on *C9ORF72* exon 2 mRNA in cytoplasm (~30%, $p < 0.05$) and no impact on the nuclear localized variants (Figure 8C). Conversely, di-siRNA 11437 significantly reduces *C9ORF72* exon 2 mRNA in both the nucleus and cytoplasm, with a larger decrease observed in the cytoplasm (Figure 8C).

Interestingly, the number of cells with *C9ORF72* exon 2 mRNA clusters appeared unchanged after either di-siRNA 136 or di-siRNA 11437 treatment (Figure 8D), suggesting that the clustered mRNA species are resistant to the degradation by the RISC machinery.

DISCUSSION

More than 10 years have passed since the original discovery of a hexanucleotide G_4C_2 expansion within intron 1 of *C9ORF72* as the leading genetic driver of ALS and FTD. Loss of function of the C9ORF72 protein is proposed to lead to haploinsufficiency, while sense and antisense transcription of the G_4C_2 expansion produces RNA that form RNA foci, and the expansion can be translated into toxic poly di-peptide repeat proteins.[7,26,35,57–62] More recently, a converging of these two hypotheses has been proposed where loss of C9ORF72 protein exacerbates toxicity from the HRE.[63,64] An effective therapeutic strategy may be to reduce the G_4C_2 expansion-containing transcripts, while maintaining the main C9ORF72 protein-producing transcript. Here, we report siRNAs with the ability to reduce *C9ORF72* transcripts in a C9-ALS/FTD mouse model. The siRNAs were designed to specifically target repeat-containing transcripts or non-selectively target all *C9ORF72* RNAs. The silencing of these transcripts is expected to be achieved through RISC-based targeting, and this has previously been shown to be specific for the target mRNA[42]; however, the specificity of this siRNA was not assessed. ICV administration of siRNA targeting exon 1 sequences displays reduction in V1/V3 transcripts without impact on overall levels of *C9ORF72* transcripts. These siRNAs also reduce RNA foci, and poly(GP) dipeptides throughout the brain. siRNA targeting exon 2 or exon 4 reduce V1/V3 transcripts as well as total *C9ORF72* RNA, and profoundly reduce both nuclear and cytoplasmic RNA and poly(GP) dipeptides throughout the brain and spinal cord. This proof-of-concept work supports the further characterization of siRNA-driven *C9ORF72* reduction, such as investigation into mRNA, RNA foci, and poly(GP) reduction in patient-derived cells, and correction of disrupted pathways after *C9ORF72* reduction in a human background.

Similar to work on other neurological diseases, such as Huntington and Alzheimer disease,[49,65] the intracellular location of the *C9ORF72* target sequence has a profound impact on the efficacy of siRNA. We find that targeting *C9ORF72* non-selectively produces greater mRNA reduction *in vitro* and *in vivo*. This may be explained by the relatively greater potency of non-selective *C9ORF72* siRNA compared to selective *C9ORF72* when targeting mRNA sequences in their native context. The highly structured RNA surrounding the HRE may impede RISC loading of target sequences; thus, sequences further away from the HRE are more accessible to siRNA-mediated silencing. This is demonstrated in a luciferase reporter assay where sequences are taken out of their native context, and siRNA targeting

Figure 5. Targeted siRNA screen around position 136 of *C9ORF72* exon 1 identifies region efficiently targetable by RNAi machinery

(A) Design of the single nucleotide siRNA walk around C9ORF72-143 (exon 1) targeting position. Exon region (upper case) and intron region (lower case). (B) Chemical configuration of siRNA used for screening. (C and D) Primary astrocytes, derived from C57BL/6J-Tg(C9orf72_i3) mice, were treated with a panel of siRNAs and levels of full-length *C9ORF72* mRNA (C), and exon 1-containing *C9ORF72* variants (D) were evaluated at 72 h (QuantiGene, $n = 3–4$, mean ± SD, one-way ANOVA, Dunnett's multiple comparison correction; $^{*}p < 0.05$; $^{**}p < 0.01$; $^{***}p < 0.001$). (E–G) Reduction of *C9ORF72* exon 1-containing variants by lead exon 1-targeting siRNA.

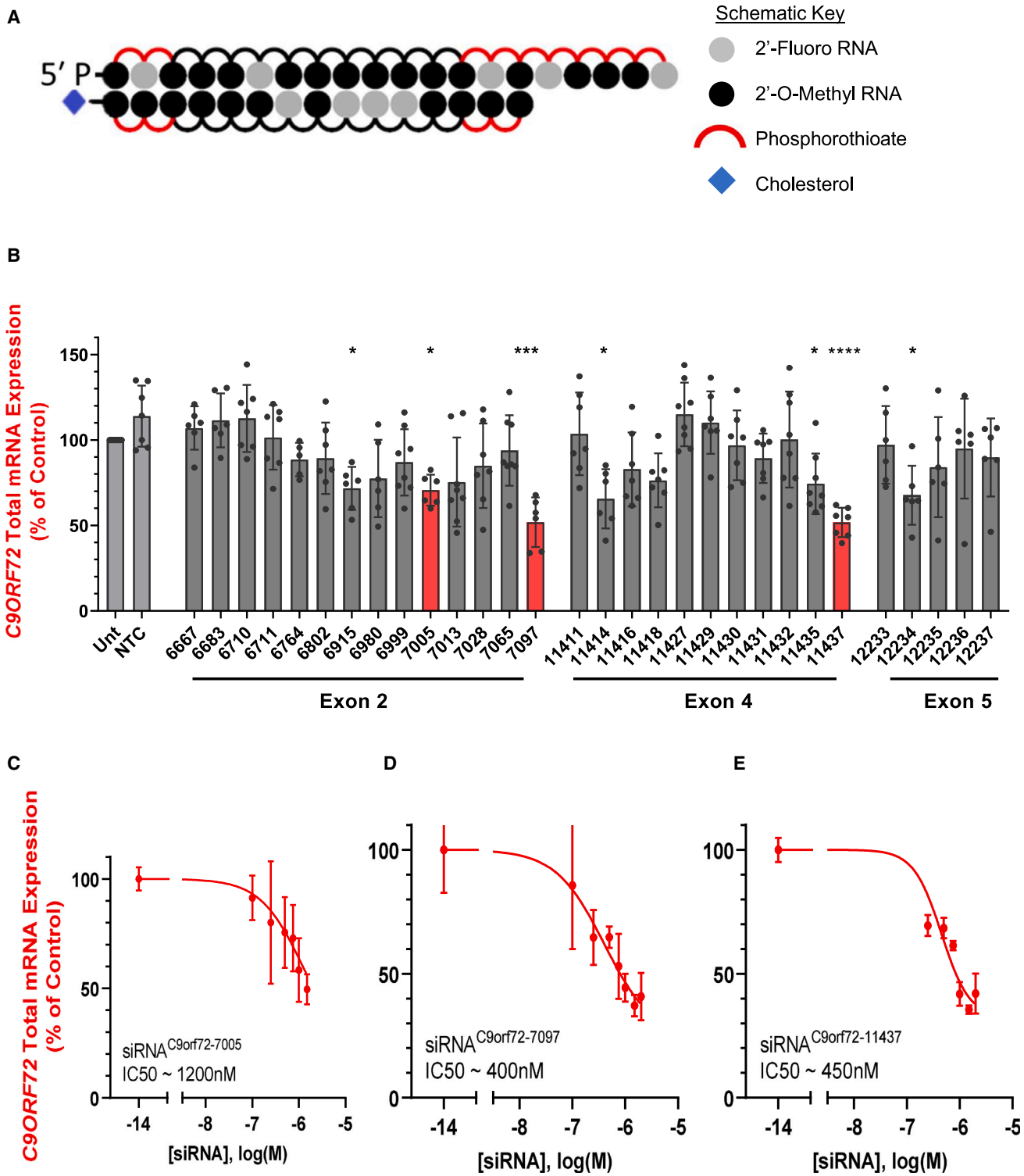

Figure 6. Broad siRNA screen across exons 2,4,5 of *C9ORF72* identifies new siRNA capable of total *C9ORF72* mRNA reduction

(A) Chemical configuration of siRNA used for screening. (B) Primary neurons, derived from C57BL/6J-Tg(C9ofr72_i3) mice, were treated with a panel siRNAs targeting C9ORF72 exon 2,4,5, and total C9ORF72 mRNA expression was assessed 72 h post-treatment (QuantiGene, n = 3–4, mean ± SD, one-way ANOVA, Dunnett's multiple comparison correction; *$p < 0.05$; **$p < 0.01$; ***$p < 0.001$). (C–E) Reduction of total *C9ORF72* mRNA by siRNA targeting C9ORF72 exon 2 and exon 4.

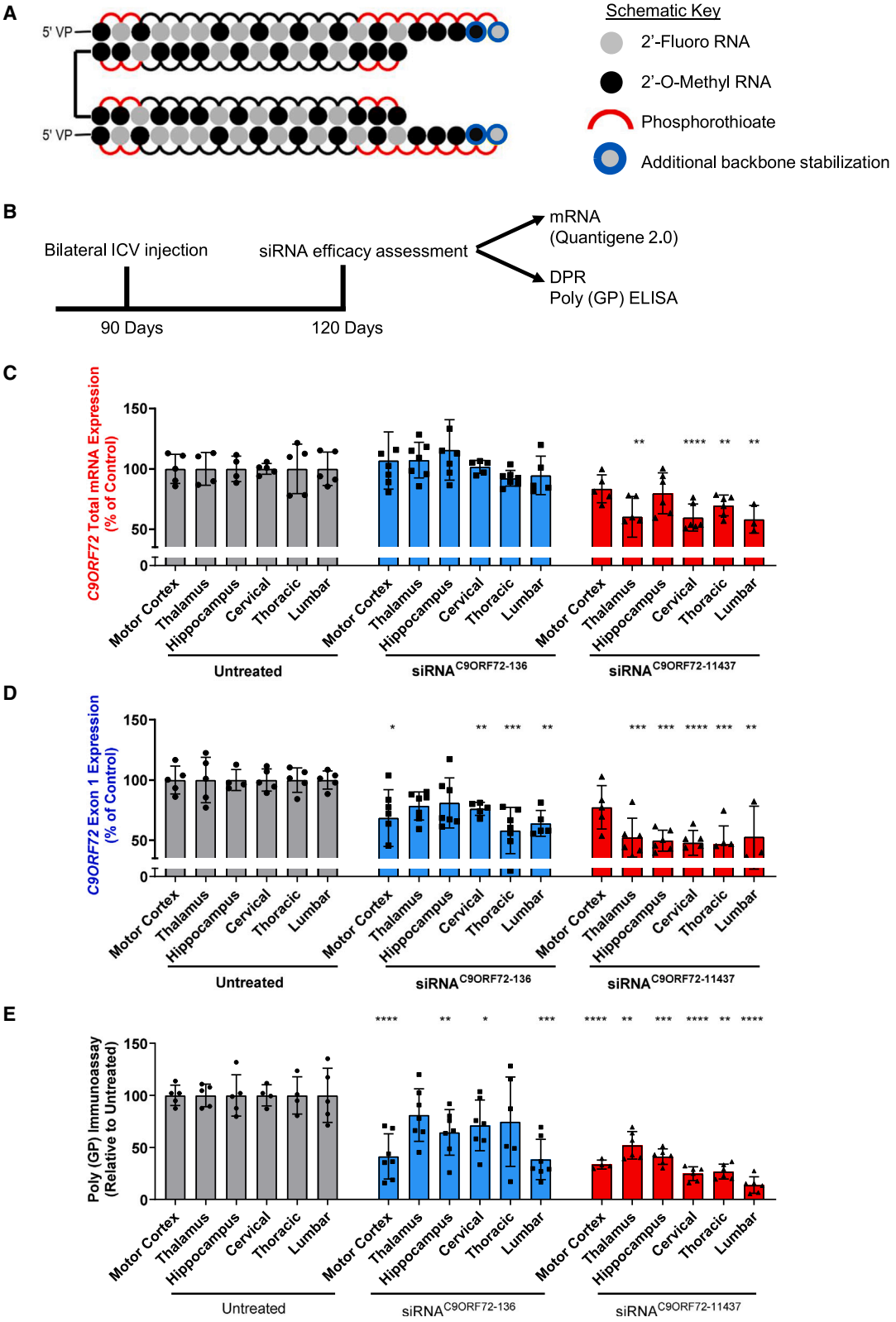

(legend on next page)

sequences 60 nt upstream of the HRE display similar potency to siRNA targeting sequences 6,000 nt downstream (siRNA 244 IC_{50}, 7 nM vs. siRNA 6686 IC_{50}, 14 nM).

Many repeat-expansion neurodegenerative diseases, including ALS and FTD, feature RNA abnormalities such as RNA foci.[7,8,66–69] In *C9ORF72*-driven ALS/FTD, transcription of the HRE is thought to form G-quadruplexes, which form RNA foci and drive disease.[70,71] Using RNAscope probes designed against exon 2 of *C9ORF72*, we find that *C9ORF72* exon 2 mRNA forms large nuclear clusters in almost half of the cells. These clusters are inaccessible to degradation and may be sequestering other RNA or protein species, driving disease. Current clinical ASOs do not target all *C9ORF72* mRNA transcripts, and this may explain the lack of clinical efficacy observed.

Early siRNA clinical trials used unmodified or partially modified oligonucleotides. These molecules failed due to extremely low stability, resulting in limited cellular delivery and on-target efficacy and unwanted activation of the immune system. To overcome these limitations, the current generation of oligonucleotide therapeutics use fully stabilized oligonucleotides.[42,72–75] To enable straightforward conversion between *in vitro* and *in vivo* experiments, all screens have been performed in the context of fully chemically stabilized siRNAs. Ribose sugars were modified with a combination of 2′-methoxy (2′-OMe) and 2′-fluoro (2′-F) ribose modification patterns, compatible with efficient RISC entry.[48,76,77] In addition, the two terminal backbone linkages are modified, with phosphorothioate providing critical additional stabilization.[78] In a context of hydrophobic conjugate, cholesterol, these architectures are efficiently internalized by all cell types, including neurons[48,79] (Figures 1D and 1E), and were used for all *in vitro* screening. The chemical scaffold from *in vitro* screening (Figure 1D) was converted to a CNS-optimized pattern used for *in vivo* assessment of siRNA efficacy, divalent siRNAs. The divalent configuration, when injected in the CSF, enable robust distribution and potent, long-lasting silencing in rodent, NHP, and sheep brains.[42,43] One enticing characteristic of oligonucleotide therapeutics including siRNA is the possibility to independently optimize the chemical scaffold and the targeting sequence. As such, the divalent siRNA scaffold used in this study can be used for any optimized target sequence, including targeting the antisense transcript of *C9ORF72*.

This manuscript describes an siRNA developed for *C9ORF72*-driven ALS and adds to the growing field of oligonucleotide therapeutics developed for CNS indications as well as *C9ORF72*. Our study provides proof of concept that siRNA can selectively reduce repeat-containing transcripts or non-selectively target all *C9ORF72* RNAs. siRNA-driven reduction of *C9ORF72* is suspected to confer the same advantages in rescuing RNA-mediated toxicity and poly-dipeptide toxicity, as has been observed with ASOs, which also target the repeat expansion directly or indirectly through targeting exon 1.[35,38] Both siRNAs and ASOs hold promise in developing treatments for *C9ORF72*-related ALS and FTD. siRNAs are generally more potent in the cytoplasm, exhibiting higher stability and prolonged efficacy. In contrast, ASOs have demonstrated better potency in modulating nuclear targets, with a wide clinical history available. Despite their advantages, ASOs may induce toxicity, including ventricular enlargements, and their effects may be less durable. Balancing these considerations, future research will need to define which combination of technologies provides the best option for developing disease-modifying treatments for ALS.

MATERIALS AND METHODS

Design of chemically modified siRNAs

We designed a panel of 118 siRNA compounds targeting the human *C9ORF72* gene. The siRNAs sequences target across *C9ORF72* exon 1, intron 1, exon 2, exon 4, and exon 5 and were designed according to previously established guidelines for siRNA design.[45] Adherence to the guidelines influenced the selection of sequences, which were target specific, contained optimal GC content, contained low seed complement frequency, removed sequences containing toxic motifs, and removed sequences containing known miRNA seeds.

Oligonucleotide synthesis

Oligonucleotides were synthesized as previously described.[48–50,79] Briefly, oligonucleotides were synthesized by phosphoramidite solid-phase synthesis on a Dr. Oligo 48 (Biolytic, Fremont, CA) or a MerMade12 (Biosearch Technologies, Novato, CA) using modified protocols. Modified 2'-F, 2'-OMe phosphoramidites with standard protecting groups were used. (ChemGenes, Wilmington, MA, and/or Hongene Biotech, Union City, CA). Bis-cyanoethyl-*N*,*N*-diisopropyl CED phosphoramidite was used for the addition of the 5′-phosphate for screen compounds (ChemGenes), and 5′-(E)-vinyl tetraphosphonate (pivaloyloxymethyl) 2′-*O*-methyl-uridine 3′-CE phosphoramidite was used for the addition of 5′-vinyl phosphonate (Hongene Biotech). Phosphoramidites were dissolved at 0.1 M in anhydrous acetonitrile (ACN), with added anhydrous 15% dimethylformamide in the case of 2′-OMe-uridine amidite. 5-(Benzylthio)-1H-tetrazole was used as the activator at 0.25 M. Detritylations were performed using 3% trichloroacetic acid in dichloromethane. The capping reagents used were CAP A (20% *N*-methylimidazole in ACN) and CAP B (20% acetic anhydride and 30% 2,6-lutidine in ACN). Phosphite oxidation to convert to phosphate or phosphorothioate was performed with 0.05 M iodine in pyridine-H_2O (9:1, v/v) or a 0.1-M solution of 3-[(dimethylaminomethylene)amino]-3H-1,2,4-dithiazole-5-thione in

Figure 7. *C9ORF72* targeting siRNA injected into a C9-ALS mouse model displays significant RNA and DPR reduction

(A) Divalent siRNA scaffold used for *in vivo* studies. (B) C57BL/6J-Tg(C9ofr72_i3) mice were treated via bilateral ICV injection with 10 nmol (240 μg) siRNAs targeting C9ORF72-136 (exon 1), C9ORF72-11437 (exon 4), or untreated. (C and D) Levels of full-length C9ORF72 mRNA (C) and exon 1-containing C9ORF72 variants (D) were evaluated by QuantiGene assay 30 days post-injection. (Expression was normalized to the housekeeping gene *Hprt*. n = 3–4, mean ± SD, one-way ANOVA; $^{*}p < 0.05$; $^{**}p < 0.01$; $^{***}p < 0.001$; $^{****}p < 0.0001$.) (E) Reduction in poly(GP) after di-siRNA treatment, quantified using MSD ELISA poly(GP) assay was assessed 30 days post-injection (n = 5, mean ± SD, one-way ANOVA, Dunnett's multiple comparison correction; $^{*}p < 0.05$; $^{**}p < 0.01$; $^{***}p < 0.001$; $^{****}p < 0.0001$).

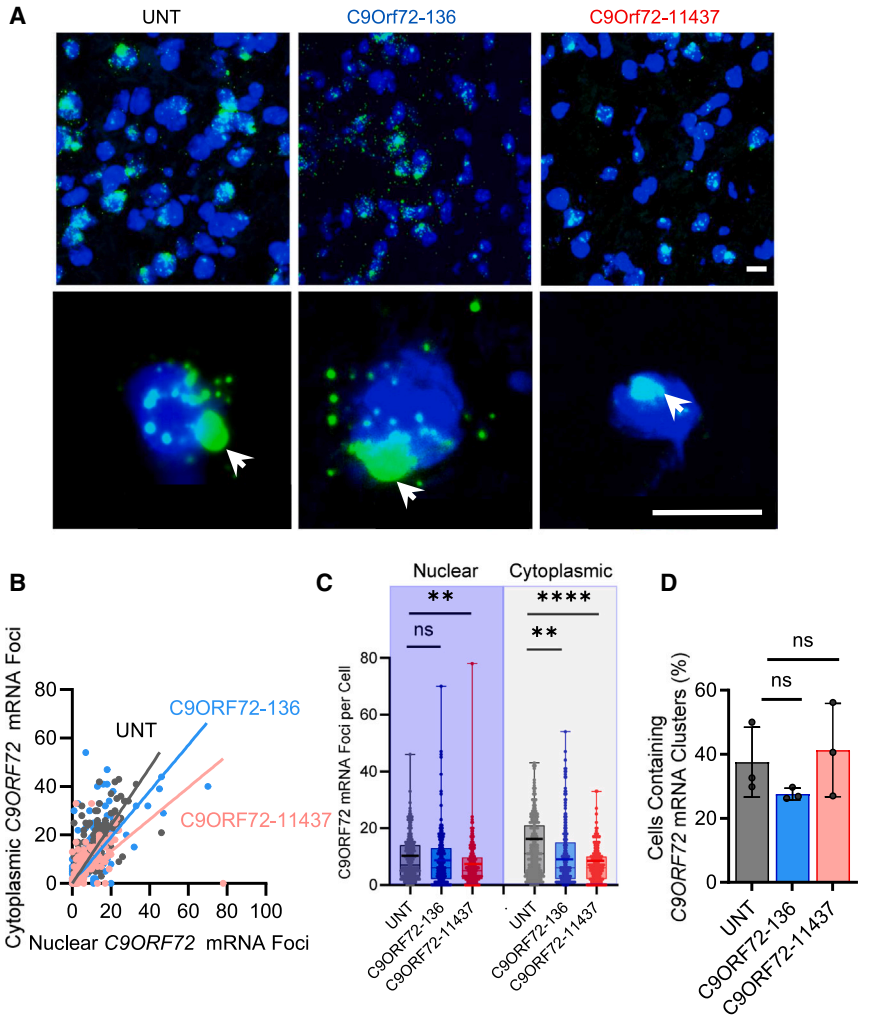

Figure 8. Intranuclear *C9ORF72* mRNA clusters but not individual foci are resistant to siRNA treatment

C57BL/6J-Tg(C9orf72_i3) mice were treated via bilateral ICV injection with 10 nmol (240 μg) siRNAs targeting C9ORF72-136 (exon 1) and C9ORF72-11437 (exon 4). Six weeks post-injection, localization of *C9ORF72* transcript was visualized by RNAscope in the thalamus (n = 3 mice, 170–220 randomly selected cells, arrows point to intranuclear mRNA clusters). (A) Representative fluorescent images, scale bar, 10 μm (green, C9ORF72 mRNA; blue, DAPI). (B) Scatterplot of nuclear and cytoplasmic foci per cell (170–220 cells per sample, n = 3 mice). (C) Reduction in cytoplasmic and nuclear foci after treatment with C9ORF72-136 or C9ORF72-11437 (n = 3 mice, 170–220 cells, one-way ANOVA, Dunnett's multiple comparison correction; $^{*}p < 0.05$; $^{**}p < 0.01$; $^{****}p < 0.0001$). (D) Reduction in the percentage of nuclei containing *C9ORF72* aggregates after treatment with C9ORF72-136 or C9ORF72-11437 (n = 3 mean ± SD). Aggregates are defined as having a larger diameter than 0.6 μm. ns, no statistical difference was observed between the samples.

pyridine purchased from ChemGenes for 3 min. Coupling times were 4 min. Reagents were purchased from American International Chemical (Westborough, MA) and/or ChemGenes. Unconjugated oligonucleotides were synthesized on 500-Å long-chain alkyl amine (LCAA) controlled pore glass (CPG) functionalized with Unylinker terminus (ChemGenes). Cholesterol-conjugated oligonucleotides were synthesized on a 500-Å LCAA-CPG support, where the cholesterol moiety is bound to tetra-ethylene glycol through a succinate linker (ChemGenes). Divalent oligonucleotides (DIOs) were synthesized on custom solid support prepared in-house.

Screen synthesis was made on a 1-μmol scale. Synthesis columns were custom packed at LGC Genomics (Alexandria, MN).

Deprotection and purification of oligonucleotides for sequence screening

Oligonucleotides used for *in vitro* experiments were deprotected with ammonia gas (Airgas Specialty Gases), and a modified on-column ethanol precipitation protocol was used for purification.

Deprotection and purification of oligonucleotides for *in vivo* experiments

Vinyl phosphonate-containing oligonucleotides were cleaved and deprotected with 3% diethylamine in ammonium hydroxide for 20 h at 35°C with slight agitation. DIOs were deprotected with 1:1 ammonium hydroxide and aqueous monomethylamine for 2 h at 25°C with slight agitation. The controlled pore glass was subsequently filtered and rinsed with 30 mL 5% ACN in water and dried overnight by centrifugal vacuum concentration. Purifications were performed on an Agilent 1290 Infinity II high-performance liquid chromatography (LC) system using Source 15Q anion exchange resin (Cytiva, Marlborough, MA). The loading solution was 20 mM sodium acetate in 10% ACN in water, and elution solution was the loading solution with 1 M sodium bromide, using a linear gradient from 30% to 70% in 40 min at 50°C. Pure fractions were combined and desalted by size exclusion with Sephadex G-25 (Cytiva).

Purity and identity of fractions and pure oligonucleotides were confirmed by ion-pair reversed-phase LC/mass spectrometry- (MS) on an Agilent 6530 Accurate-mass QTOF LC/MS.

Quantigene 2.0 probes

Quantigene 2.0 probes against total *C9ORF72* are available for purchase through Thermo Fisher Scientific (assay ID: SA-3015063). These probes capture mRNA through C9ORF72 exon 2 and detect through exons 2–4. Quantigene 2.0 probes against exon 1 *C9ORF72* were custom ordered and captured mRNA through C9ORF72 exon 2 and detected through exon 1.

Cell culture for luciferase assays

HeLa cells (American Type Culture Collection CCL-2) were maintained in DMEM (Thermo Fisher) supplemented with 10% fetal bovine serum (FBS; Gibco) and 100 U/mL penicillin/streptomycin (Invitrogen, Waltham, MA). HeLa cells were grown at 37°C and 5% CO_2 and passaged every 2–5 days. Three days prior to treatment, 10-cm^2 dishes were plated with 2×10^6 HeLa cells and grown overnight. The following day, DMEM was replaced with serum-free OptiMEM (Gibco) containing 20 μg reporter plasmid and 60 μL Lipofectamine 2000 (Invitrogen). Following a 20-min incubation, this solution was added dropwise to the dish containing HeLa cells. The cells were incubated for 6 h, before washing with PBS and placed in DMEM with 10% FBS overnight. The following day, 50 μL HeLa cells previously transfected with reporter plasmid were transferred to a 96-well white wall clear bottom tissue culture plate and treated with siRNA conjugated to cholesterol. This conjugation method negates the need for other transfection reagents. After 72 h of treatment, cells were washed twice with PBS, then lysed with 50 μL Dual-Glo reagent. After 15 min, luminescence was read on a luminometer. A total of 50 μL Dual-Glo Stop & Glo reagent was added, followed by another 15-min incubation before the assessment of *Renilla* luminescence. Luminescence values were normalized to untreated controls.

Preparation of primary neurons

Primary cortical neurons and astrocytes were obtained following previously described protocols.[80] Embryos were isolated from embryonic day 15 heterozygous C57BL/6J-g(*C9ORF72*_i3)112Lutzy/J mice. Pregnant C57BL/6J females were anesthetized via inhalation of isoflurane, followed by cervical dislocation. Embryos were removed and transferred to a Petri dish containing cold DMEM. Brains were removed from embryos and meninges detached. Following cortical isolation, brain tissue was mechanically disrupted using a fire-polished pipette tip for neurons or surgical scalpel for astrocytes.

Cortices designated for neuron preparation were transferred to prewarmed papain/DNAse solution and incubated for 30 min. Following rounds of gentle dissociation, neurons were counted using a hemocytometer, and 100 μL containing 1×10^5 of neurons was transferred to each well of a poly-L-lysine precoated 96-well plate. The following day, 100 μL medium containing anti-mitotics was added to each well, and every subsequent 2–3 days, half of the volume of media was replaced with freshly prepared medium.

Preparation of primary astrocytes

Following cortical isolation, cortices were placed in 1.5 mL TrypLE and incubated for 25 min at 37°C and 5% CO_2. The cortices were then resuspended in 5 mL DMEM containing 10% FBS and centrifuged at 1,500 rpm for 5 min. The cellular pellet was resuspended in DMEM supplemented with 10% FBS and 10 ng/μL of mouse epidermal growth factor and added to T75 growth flasks. Dividing primary astrocytes were split every 4–5 days and discarded after 7 passages.

Delivery of siRNA through passive uptake

Cells were plated in appropriate culture media in 96-well tissue culture plates. siRNA was diluted to twice the desired final concentration in OptiMEM (Gibco). siRNA used in all *in vitro* experiments were siRNA conjugated to cholesterol. This conjugation method negates the need for other transfection reagents. A total of 50 μL siRNA was added to 50 μL cells. For HeLa cells maintained in FBS, plating cells in 6%, which results in a final 3% FBS in the media is important. Cells for reporter assays or astrocyte assays were incubated for 72 h at 37°C and 5% CO_2. Primary neurons were incubated with siRNA for 7 days. All primary screens were performed at a 1.5-μM compound dose.

Quantification of mRNA silencing in cells

mRNA and mRNA silencing was quantified using the QuantiGene 2.0 assay (Affymetrix, Santa Clara, CA), as previously described.[80] Cell lysate was prepared and applied to plates precoated with mRNA-specific probes: mouse HPRT (SB-15463), human total *C9ORF72* (SA-3015063), and human C9ROF72 exon 1 specific (SA-6000878). Following overnight incubation, three wash and amplification steps were performed before detection on a luminometer.

Stereotactic ICV injections

All experimental studies involving animals were approved by the University of Massachusetts Chan Medical School Institutional Animal Care and Use Committee (protocol no. PROTO202000010 [A-2411]) and performed according to the guidelines and regulations described therein.

A total of 10 μL divalent siRNA was administered bilaterally (5 μL per ventricle) into the lateral ventricles of mice using a slight adaptation to a protocol previously described.[42] Briefly, mice were anesthetized using isoflurane and maintained under isoflurane during the procedure. After the identification of bregma, stereotaxic devices were used to inject siRNA at coordinates from bregma: −0.2 mm anteroposterior, ±0.8 mm mediolateral, and and −2.5 mm dorsoventral. Injections were performed at 1,000 nL/min. Following completion of the injection, the mice received saline and subcutaneous meloxicam SR at 4 mg/kg and were monitored until fully ambulatory.

Collection of tissue

Mice were euthanized using isoflurane overdose followed by bilateral pneumothorax. Following harvesting, tissues were either flash-frozen or stored in RNALater (Invitrogen). Brains were sectioned prior to storage using a brain mold that allowed for creation of 1-mm-thick slices. These slices were then sectioned using a 2-mm biopsy punch to produce region-specific tissue samples. Spinal cords were flushed from the spinal column using PBS and sectioned into regions (cervical, thoracic, lumbar) before being stored.

Quantification of mRNA silencing in tissue

Tissue collected for mRNA and mRNA silencing was quantified using the QuantiGene 2.0 Assay (Affymetrix). Tissue punches stored in RNAlater or flash-frozen were homogenized in QuantiGene 2.0

homogenizing buffer (Invitrogen) with proteinase K (Invitrogen) using mechanical dissociation. Following incubation at 55°C for 1 h, lysate was used as described for the quantification of mRNA from cells.

Quantification of DPR protein in tissue

Tissue punches were collected as above and flash-frozen and placed at −80 C. After addition of radioimmunoprecipitation assay buffer with protease inhibitors, samples were homogenized and quantified through Pierce BCA protein sssay (Thermo Fisher). Custom capture antibody to poly(GP) generated and generously shared by Dr Robert Brown's lab at UMass Chan Medical School was added to each well of a 96-well Meso Scale Discovery (MSD) ELISA plate. Following overnight incubation at 4°C, the plate was washed, incubated with PBS + 0.1% Tween, and incubated for 1 h. After washing, 50 µg sample in 150 µL PBS + 0.1% Tween plus standards were incubated for at least 2 h. The plate was washed once more and detected immediately on an MSD plate reader.

RNAscope fluorescence *in situ* hybridization analysis of C9ORF72 RNA aggregates

RNAscope (Bio-Techne, Minneapolis, MN) was used to visualize *C9ORF72* RNA abundance, nuclear/cytoplasmic localization, and aggregations in cultured astrocytes and fresh-frozen mouse brain sections. For astrocytes, cell cultures were prepared according to the manufacturer's protocols for cultured adherent cells. Probes detecting full-length mouse *C9orf72* (catalog no. 895781), full-length human *C9ORF72* (catalog no. 895771), and intron 1 of human *C9ORF72* (catalog no. 410291) were used to visualize aggregated and unaggregated RNA. Housekeeping gene *Hprt* (catalog no. 442881) served as a staining quality control. Images were acquired using a Leica SP8 point-scanning confocal microscope (Leica Microsystems, Wetzlar, Germany). An ImageJ-based analytical algorithm[79] was used to compute cytoplasmic and nuclear foci abundance. Colocalization analysis was computed manually and reported as number of mRNA clusters that contained both *C9ORF72* full length and *C9ORF72* intron 1 signal. Colocalization between *Hprt* and intron 1 after the intron 1 channel was rotated served as baseline controls.

For frozen brain sections, one hemisphere of the brain was frozen in optimal cutting temperature compound and cut into 10-µm sections using a cryostat. Sections containing thalamic regions were prepared for RNAscope according to the manufacturer's protocols. Probes detecting the full-length C9ORF72 (catalog no. 895771) were used to visualize C9ORF72 individual and aggregate RNA. Images were acquired using the Andor Dragonfly 200 spinning disk confocal microscope (Oxford Instruments, Concord, MA). A modified ImageJ-based analytical algorithm was used to compute nuclear foci abundance, foci per cell, and number of cells containing C9ORF72 clusters.

DATA AND CODE AVAILABILITY

All data presented in the main text and the supplemental information are available from the corresponding author upon request.

SUPPLEMENTAL INFORMATION

Supplemental information can be found online at https://doi.org/10.1016/j.omtn.2024.102291.

ACKNOWLEDGMENTS

This work was supported by NIH grants NS104022 and S10ODO20012.

AUTHOR CONTRIBUTIONS

J.W.G., B.M.D.C.G., and A.K. conceived ideas or the experimental design of the study. J.W.G., Z.K., A.S., A.W., and H.T. performed experiments/data collection. D.E., B.B., N.M., D.C., K.Y., and M.H. performed the oligonucleotide synthesis. J.W.G., Z.K., and B.M.D.C.G., performed the data analysis/interpretation. F.B.G. and R.H.B. provided revisions to the scientific content of the manuscript. J.W.G. is the primary author. A.K. is the principal investigator.

DECLARATION OF INTERESTS

J.W.G., B.MDC.G., and A.K. are named as inventors on a patent application filed (OLIGONUCLEOTIDE-BASED MODULATION OF C9orf72). A.K. is a founder of Atalanta Therapeutics.

REFERENCES

1. Chio, A., Moglia, C., Canosa, A., Manera, U., Vasta, R., Brunetti, M., Barberis, M., Corrado, L., D'Alfonso, S., Bersano, E., et al. (2019). Cognitive impairment across ALS clinical stages in a population-based cohort. Neurology *93*, e984–e994. https://doi.org/10.1212/WNL.0000000000008063.

2. Burrell, J.R., Kiernan, M.C., Vucic, S., and Hodges, J.R. (2011). Motor neuron dysfunction in frontotemporal dementia. Brain *134*, 2582–2594. https://doi.org/10.1093/brain/awr195.

3. GBD 2019 Diseases and Injuries Collaborators (2020). Global burden of 369 diseases and injuries in 204 countries and territories, 1990-2019: a systematic analysis for the Global Burden of Disease Study 2019. Lancet *396*, 1204–1222. https://doi.org/10.1016/S0140-6736(20)30925-9.

4. Lacomblez, L., Bensimon, G., Leigh, P.N., Guillet, P., Powe, L., Durrleman, S., Delumeau, J.C., and Meininger, V. (1996). A confirmatory dose-ranging study of riluzole in ALS. ALS/Riluzole Study Group-II. Neurology *47*, S242–S250. https://doi.org/10.1212/wnl.47.6_suppl_4.242s.

5. Witzel, S., Maier, A., Steinbach, R., Grosskreutz, J., Koch, J.C., Sarikidi, A., Petri, S., Günther, R., Wolf, J., Hermann, A., et al. (2022). Safety and Effectiveness of Long-term Intravenous Administration of Edaravone for Treatment of Patients With Amyotrophic Lateral Sclerosis. JAMA Neurol. *79*, 121–130. https://doi.org/10.1001/jamaneurol.2021.4893.

6. Paganoni, S., Hendrix, S., Dickson, S.P., Knowlton, N., Macklin, E.A., Berry, J.D., Elliott, M.A., Maiser, S., Karam, C., Caress, J.B., et al. (2021). Long-term survival of participants in the CENTAUR trial of sodium phenylbutyrate-taurursodiol in amyotrophic lateral sclerosis. Muscle Nerve *63*, 31–39. https://doi.org/10.1002/mus.27091.

7. DeJesus-Hernandez, M., Mackenzie, I.R., Boeve, B.F., Boxer, A.L., Baker, M., Rutherford, N.J., Nicholson, A.M., Finch, N.A., Flynn, H., Adamson, J., et al. (2011). Expanded GGGGCC hexanucleotide repeat in noncoding region of C9ORF72 causes chromosome 9p-linked FTD and ALS. Neuron *72*, 245–256. https://doi.org/10.1016/j.neuron.2011.09.011.

8. Renton, A.E., Majounie, E., Waite, A., Simón-Sánchez, J., Rollinson, S., Gibbs, J.R., Schymick, J.C., Laaksovirta, H., van Swieten, J.C., Myllykangas, L., et al. (2011). A hexanucleotide repeat expansion in C9ORF72 is the cause of chromosome 9p21-linked ALS-FTD. Neuron *72*, 257–268. https://doi.org/10.1016/j.neuron.2011.09.010.

9. van der Zee, J., Gijselinck, I., Dillen, L., Van Langenhove, T., Theuns, J., Engelborghs, S., Philtjens, S., Vandenbulcke, M., Sleegers, K., Sieben, A., et al. (2013). A pan-European study of the C9orf72 repeat associated with FTLD: geographic prevalence,

genomic instability, and intermediate repeats. Hum. Mutat. *34*, 363–373. https://doi.org/10.1002/humu.22244.

10. Brown, C.A., Lally, C., Kupelian, V., and Flanders, W.D. (2021). Estimated Prevalence and Incidence of Amyotrophic Lateral Sclerosis and SOD1 and C9orf72 Genetic Variants. Neuroepidemiology *55*, 342–353. https://doi.org/10.1159/000516752.

11. Byrne, S., Elamin, M., Bede, P., Shatunov, A., Walsh, C., Corr, B., Heverin, M., Jordan, N., Kenna, K., Lynch, C., et al. (2012). Cognitive and clinical characteristics of patients with amyotrophic lateral sclerosis carrying a C9orf72 repeat expansion: a population-based cohort study. Lancet Neurol. *11*, 232–240. https://doi.org/10.1016/S1474-4422(12)70014-5.

12. Liu, E.Y., Russ, J., Wu, K., Neal, D., Suh, E., McNally, A.G., Irwin, D.J., Van Deerlin, V.M., and Lee, E.B. (2014). C9orf72 hypermethylation protects against repeat expansion-associated pathology in ALS/FTD. Acta Neuropathol. *128*, 525–541. https://doi.org/10.1007/s00401-014-1286-y.

13. O'Rourke, J.G., Bogdanik, L., Yáñez, A., Lall, D., Wolf, A.J., Muhammad, A.K.M.G., Ho, R., Carmona, S., Vit, J.P., Zarrow, J., et al. (2016). C9orf72 is required for proper macrophage and microglial function in mice. Science *351*, 1324–1329. https://doi.org/10.1126/science.aaf1064.

14. Sellier, C., Campanari, M.L., Julie Corbier, C., Gaucherot, A., Kolb-Cheynel, I., Oulad-Abdelghani, M., Ruffenach, F., Page, A., Ciura, S., Kabashi, E., and Charlet-Berguerand, N. (2016). Loss of C9ORF72 impairs autophagy and synergizes with polyQ Ataxin-2 to induce motor neuron dysfunction and cell death. EMBO J. *35*, 1276–1297. https://doi.org/10.15252/embj.201593350.

15. Sullivan, P.M., Zhou, X., Robins, A.M., Paushter, D.H., Kim, D., Smolka, M.B., and Hu, F. (2016). The ALS/FTLD associated protein C9orf72 associates with SMCR8 and WDR41 to regulate the autophagy-lysosome pathway. Acta Neuropathol. Commun. *4*, 51. https://doi.org/10.1186/s40478-016-0324-5.

16. Ugolino, J., Ji, Y.J., Conchina, K., Chu, J., Nirujogi, R.S., Pandey, A., Brady, N.R., Hamacher-Brady, A., and Wang, J. (2016). Loss of C9orf72 Enhances Autophagic Activity via Deregulated mTOR and TFEB Signaling. PLoS Genet. *12*, e1006443. https://doi.org/10.1371/journal.pgen.1006443.

17. Shao, Q., Yang, M., Liang, C., Ma, L., Zhang, W., Jiang, Z., Luo, J., Lee, J.K., Liang, C., and Chen, J.F. (2020). C9orf72 and smcr8 mutant mice reveal MTORC1 activation due to impaired lysosomal degradation and exocytosis. Autophagy *16*, 1635–1650. https://doi.org/10.1080/15548627.2019.1703353.

18. Wang, M., Wang, H., Tao, Z., Xia, Q., Hao, Z., Prehn, J.H.M., Zhen, X., Wang, G., and Ying, Z. (2020). C9orf72 associates with inactive Rag GTPases and regulates mTORC1-mediated autophagosomal and lysosomal biogenesis. Aging Cell *19*, e13126. https://doi.org/10.1111/acel.13126.

19. Belzil, V.V., Bauer, P.O., Prudencio, M., Gendron, T.F., Stetler, C.T., Yan, I.K., Pregent, L., Daughrity, L., Baker, M.C., Rademakers, R., et al. (2013). Reduced C9orf72 gene expression in c9FTD/ALS is caused by histone trimethylation, an epigenetic event detectable in blood. Acta Neuropathol. *126*, 895–905. https://doi.org/10.1007/s00401-013-1199-1.

20. Xi, Z., Zinman, L., Moreno, D., Schymick, J., Liang, Y., Sato, C., Zheng, Y., Ghani, M., Dib, S., Keith, J., et al. (2013). Hypermethylation of the CpG island near the G4C2 repeat in ALS with a C9orf72 expansion. Am. J. Hum. Genet. *92*, 981–989. https://doi.org/10.1016/j.ajhg.2013.04.017.

21. Shi, Y., Lin, S., Staats, K.A., Li, Y., Chang, W.H., Hung, S.T., Hendricks, E., Linares, G.R., Wang, Y., Son, E.Y., et al. (2018). Haploinsufficiency leads to neurodegeneration in C9ORF72 ALS/FTD human induced motor neurons. Nat. Med. *24*, 313–325. https://doi.org/10.1038/nm.4490.

22. Koppers, M., Blokhuis, A.M., Westeneng, H.J., Terpstra, M.L., Zundel, C.A.C., Vieira de Sá, R., Schellevis, R.D., Waite, A.J., Blake, D.J., Veldink, J.H., et al. (2015). C9orf72 ablation in mice does not cause motor neuron degeneration or motor deficits. Ann. Neurol. *78*, 426–438. https://doi.org/10.1002/ana.24453.

23. Sudria-Lopez, E., Koppers, M., de Wit, M., van der Meer, C., Westeneng, H.J., Zundel, C.A.C., Youssef, S.A., Harkema, L., de Bruin, A., Veldink, J.H., et al. (2016). Full ablation of C9orf72 in mice causes immune system-related pathology and neoplastic events but no motor neuron defects. Acta Neuropathol. *132*, 145–147. https://doi.org/10.1007/s00401-016-1581-x.

24. Cooper-Knock, J., Walsh, M.J., Higginbottom, A., Robin Highley, J., Dickman, M.J., Edbauer, D., Ince, P.G., Wharton, S.B., Wilson, S.A., Kirby, J., et al. (2014). Sequestration of multiple RNA recognition motif-containing proteins by C9orf72 repeat expansions. Brain *137*, 2040–2051. https://doi.org/10.1093/brain/awu120.

25. Zhang, K., Donnelly, C.J., Haeusler, A.R., Grima, J.C., Machamer, J.B., Steinwald, P., Daley, E.L., Miller, S.J., Cunningham, K.M., Vidensky, S., et al. (2015). The C9orf72 repeat expansion disrupts nucleocytoplasmic transport. Nature *525*, 56–61. https://doi.org/10.1038/nature14973.

26. Ash, P.E.A., Bieniek, K.F., Gendron, T.F., Caulfield, T., Lin, W.L., Dejesus-Hernandez, M., van Blitterswijk, M.M., Jansen-West, K., Paul, J.W., Rademakers, R., et al. (2013). Unconventional translation of C9ORF72 GGGGCC expansion generates insoluble polypeptides specific to c9FTD/ALS. Neuron *77*, 639–646. https://doi.org/10.1016/j.neuron.2013.02.004.

27. Kanekura, K., Yagi, T., Cammack, A.J., Mahadevan, J., Kuroda, M., Harms, M.B., Miller, T.M., and Urano, F. (2016). Poly-dipeptides encoded by the C9ORF72 repeats block global protein translation. Hum. Mol. Genet. *25*, 1803–1813. https://doi.org/10.1093/hmg/ddw052.

28. Lopez-Gonzalez, R., Lu, Y., Gendron, T.F., Karydas, A., Tran, H., Yang, D., Petrucelli, L., Miller, B.L., Almeida, S., and Gao, F.B. (2016). Poly(GR) in C9ORF72-Related ALS/FTD Compromises Mitochondrial Function and Increases Oxidative Stress and DNA Damage in iPSC-Derived Motor Neurons. Neuron *92*, 383–391. https://doi.org/10.1016/j.neuron.2016.09.015.

29. Zhang, Y.J., Gendron, T.F., Grima, J.C., Sasaguri, H., Jansen-West, K., Xu, Y.F., Katzman, R.B., Gass, J., Murray, M.E., Shinohara, M., et al. (2016). C9ORF72 poly(GA) aggregates sequester and impair HR23 and nucleocytoplasmic transport proteins. Nat. Neurosci. *19*, 668–677. https://doi.org/10.1038/nn.4272.

30. Shi, K.Y., Mori, E., Nizami, Z.F., Lin, Y., Kato, M., Xiang, S., Wu, L.C., Ding, M., Yu, Y., Gall, J.G., and McKnight, S.L. (2017). Toxic PRn poly-dipeptides encoded by the C9orf72 repeat expansion block nuclear import and export. Proc. Natl. Acad. Sci. USA *114*, E1111–E1117. https://doi.org/10.1073/pnas.1620293114.

31. Zhang, Y.J., Gendron, T.F., Ebbert, M.T.W., O'Raw, A.D., Yue, M., Jansen-West, K., Zhang, X., Prudencio, M., Chew, J., Cook, C.N., et al. (2018). Poly(GR) impairs protein translation and stress granule dynamics in C9orf72-associated frontotemporal dementia and amyotrophic lateral sclerosis. Nat. Med. *24*, 1136–1142. https://doi.org/10.1038/s41591-018-0071-1.

32. Shao, Q., Liang, C., Chang, Q., Zhang, W., Yang, M., and Chen, J.F. (2019). C9orf72 deficiency promotes motor deficits of a C9ALS/FTD mouse model in a dose-dependent manner. Acta Neuropathol. Commun. *7*, 32. https://doi.org/10.1186/s40478-019-0685-7.

33. Zhu, Q., Jiang, J., Gendron, T.F., McAlonis-Downes, M., Jiang, L., Taylor, A., Diaz Garcia, S., Ghosh Dastidar, S., Rodriguez, M.J., King, P., et al. (2020). Reduced C9ORF72 function exacerbates gain of toxicity from ALS/FTD-causing repeat expansion in C9orf72. Nat. Neurosci. *23*, 615–624. https://doi.org/10.1038/s41593-020-0619-5.

34. Crooke, S.T., Witztum, J.L., Bennett, C.F., and Baker, B.F. (2018). RNA-Targeted Therapeutics. Cell Metabol. *27*, 714–739. https://doi.org/10.1016/j.cmet.2018.03.004.

35. Donnelly, C.J., Zhang, P.W., Pham, J.T., Haeusler, A.R., Mistry, N.A., Vidensky, S., Daley, E.L., Poth, E.M., Hoover, B., Fines, D.M., et al. (2013). RNA toxicity from the ALS/FTD C9ORF72 expansion is mitigated by antisense intervention. Neuron *80*, 415–428. https://doi.org/10.1016/j.neuron.2013.10.015.

36. Lagier-Tourenne, C., Baughn, M., Rigo, F., Sun, S., Liu, P., Li, H.R., Jiang, J., Watt, A.T., Chun, S., Katz, M., et al. (2013). Targeted degradation of sense and antisense C9orf72 RNA foci as therapy for ALS and frontotemporal degeneration. Proc. Natl. Acad. Sci. USA *110*, E4530–E4539. https://doi.org/10.1073/pnas.1318835110.

37. Jiang, J., Zhu, Q., Gendron, T.F., Saberi, S., McAlonis-Downes, M., Seelman, A., Stauffer, J.E., Jafar-Nejad, P., Drenner, K., Schulte, D., et al. (2016). Gain of Toxicity from ALS/FTD-Linked Repeat Expansions in C9ORF72 Is Alleviated by Antisense Oligonucleotides Targeting GGGGCC-Containing RNAs. Neuron *90*, 535–550. https://doi.org/10.1016/j.neuron.2016.04.006.

38. Liu, Y., Dodart, J.C., Tran, H., Berkovitch, S., Braun, M., Byrne, M., Durbin, A.F., Hu, X.S., Iwamoto, N., Jang, H.G., et al. (2021). Variant-selective stereopure oligonucleotides protect against pathologies associated with C9orf72-repeat expansion in preclinical models. Nat. Commun. *12*, 847. https://doi.org/10.1038/s41467-021-21112-8.

39. Tran, H., Moazami, M.P., Yang, H., McKenna-Yasek, D., Douthwright, C.L., Pinto, C., Metterville, J., Shin, M., Sanil, N., Dooley, C., et al. (2022). Suppression of mutant

C9orf72 expression by a potent mixed backbone antisense oligonucleotide. Nat. Med. *28*, 117–124. https://doi.org/10.1038/s41591-021-01557-6.

40. Sciences, W.L. (2022). Study of WVE-004 in Patients With C9orf72-associated Amyotrophic Lateral Sclerosis (ALS) or Frontotemporal Dementia (FTD) (FOCUS-C9). https://clinicaltrials.gov/ct2/show/NCT04931862?term=WVE-004&draw=2&rank=1.

41. Biogen (2022). Biogen and Ionis Announce Topline Phase 1 Study Results of Investigational Drug in C9orf72 Amyotrophic Lateral Sclerosis. https://investors.biogen.com/news-releases/news-release-details/biogen-and-ionis-announce-topline-phase-1-study-results.

42. Alterman, J.F., Godinho, B.M.D.C., Hassler, M.R., Ferguson, C.M., Echeverria, D., Sapp, E., Haraszti, R.A., Coles, A.H., Conroy, F., Miller, R., et al. (2019). A divalent siRNA chemical scaffold for potent and sustained modulation of gene expression throughout the central nervous system. Nat. Biotechnol. *37*, 884–894. https://doi.org/10.1038/s41587-019-0205-0.

43. Ferguson, C.M., Godinho, B.M., Alterman, J.F., Coles, A.H., Hassler, M., Echeverria, D., Gilbert, J.W., Knox, E.G., Caiazzi, J., Haraszti, R.A., et al. (2021). Comparative route of administration studies using therapeutic siRNAs show widespread gene modulation in Dorset sheep. JCI Insight *6*, e152203. https://doi.org/10.1172/jci.insight.152203.

44. Tran, H., Almeida, S., Moore, J., Gendron, T.F., Chalasani, U., Lu, Y., Du, X., Nickerson, J.A., Petrucelli, L., Weng, Z., and Gao, F.B. (2015). Differential Toxicity of Nuclear RNA Foci versus Dipeptide Repeat Proteins in a Drosophila Model of C9ORF72 FTD/ALS. Neuron *87*, 1207–1214. https://doi.org/10.1016/j.neuron.2015.09.015.

45. Birmingham, A., Anderson, E., Sullivan, K., Reynolds, A., Boese, Q., Leake, D., Karpilow, J., and Khvorova, A. (2007). A protocol for designing siRNAs with high functionality and specificity. Nat. Protoc. *2*, 2068–2078. https://doi.org/10.1038/nprot.2007.278.

46. O'Rourke, J.G., Bogdanik, L., Muhammad, A.K.M.G., Gendron, T.F., Kim, K.J., Austin, A., Cady, J., Liu, E.Y., Zarrow, J., Grant, S., et al. (2015). C9orf72 BAC Transgenic Mice Display Typical Pathologic Features of ALS/FTD. Neuron *88*, 892–901. https://doi.org/10.1016/j.neuron.2015.10.027.

47. Tang, Q., Sousa, J., Echeverria, D., Fan, X., Hsueh, Y.C., Afshari, K., MeHugh, N., Cooper, D.A., Vangjeli, L., Monopoli, K., et al. (2022). RNAi-based modulation of IFN-gamma signaling in skin. Mol. Ther. *30*, 2709–2721. https://doi.org/10.1016/j.ymthe.2022.04.019.

48. Alterman, J.F., Hall, L.M., Coles, A.H., Hassler, M.R., Didiot, M.C., Chase, K., Abraham, J., Sottosanti, E., Johnson, E., Sapp, E., et al. (2015). Hydrophobically Modified siRNAs Silence Huntingtin mRNA in Primary Neurons and Mouse Brain. Mol. Ther. Nucleic Acids *4*, e266. https://doi.org/10.1038/mtna.2015.38.

49. Ferguson, C.M., Echeverria, D., Hassler, M., Ly, S., and Khvorova, A. (2020). Cell Type Impacts Accessibility of mRNA to Silencing by RNA Interference. Mol. Ther. Nucleic Acids *21*, 384–393. https://doi.org/10.1016/j.omtn.2020.06.006.

50. Conroy, F., Miller, R., Alterman, J.F., Hassler, M.R., Echeverria, D., Godinho, B.M.D.C., Knox, E.G., Sapp, E., Sousa, J., Yamada, K., et al. (2022). Chemical engineering of therapeutic siRNAs for allele-specific gene silencing in Huntington's disease models. Nat. Commun. *13*, 5802. https://doi.org/10.1038/s41467-022-33061-x.

51. Davis, S.M., Sousa, J., Vangjeli, L., Hassler, M.R., Echeverria, D., Knox, E., Turanov, A.A., Alterman, J.F., and Khvorova, A. (2020). 2'-O-Methyl at 20-mer Guide Strand 3' Termini May Negatively Affect Target Silencing Activity of Fully Chemically Modified siRNA. Mol. Ther. Nucleic Acids *21*, 266–277. https://doi.org/10.1016/j.omtn.2020.05.010.

52. Shmushkovich, T., Monopoli, K.R., Homsy, D., Leyfer, D., Betancur-Boissel, M., Khvorova, A., and Wolfson, A.D. (2018). Functional features defining the efficacy of cholesterol-conjugated, self-deliverable, chemically modified siRNAs. Nucleic Acids Res. *46*, 10905–10916. https://doi.org/10.1093/nar/gky745.

53. Takahashi, M., Suzuki, M., Fukuoka, M., Fujikake, N., Watanabe, S., Murata, M., Wada, K., Nagai, Y., and Hohjoh, H. (2015). Normalization of Overexpressed alpha-Synuclein Causing Parkinson's Disease By a Moderate Gene Silencing With RNA Interference. Mol. Ther. Nucleic Acids *4*, e241. https://doi.org/10.1038/mtna.2015.14.

54. Yamada, K., Hildebrand, S., Davis, S.M., Miller, R., Conroy, F., Sapp, E., Caiazzi, J., Alterman, J.F., Roux, L., Echeverria, D., et al. (2021). Structurally constrained phosphonate internucleotide linkage impacts oligonucleotide-enzyme interaction, and modulates siRNA activity and allele specificity. Nucleic Acids Res. *49*, 12069–12088. https://doi.org/10.1093/nar/gkab1126.

55. Parmar, R., Willoughby, J.L.S., Liu, J., Foster, D.J., Brigham, B., Theile, C.S., Charisse, K., Akinc, A., Guidry, E., Pei, Y., et al. (2016). 5'-(E)-Vinylphosphonate: A Stable Phosphate Mimic Can Improve the RNAi Activity of siRNA-GalNAc Conjugates. Chembiochem *17*, 985–989. https://doi.org/10.1002/cbic.201600130.

56. Haraszti, R.A., Roux, L., Coles, A.H., Turanov, A.A., Alterman, J.F., Echeverria, D., Godinho, B.M.D.C., Aronin, N., and Khvorova, A. (2017). 5-Vinylphosphonate improves tissue accumulation and efficacy of conjugated siRNAs in vivo. Nucleic Acids Res. *45*, 7581–7592. https://doi.org/10.1093/nar/gkx507.

57. Mizielinska, S., Lashley, T., Norona, F.E., Clayton, E.L., Ridler, C.E., Fratta, P., and Isaacs, A.M. (2013). C9orf72 frontotemporal lobar degeneration is characterised by frequent neuronal sense and antisense RNA foci. Acta Neuropathol. *126*, 845–857. https://doi.org/10.1007/s00401-013-1200-z.

58. Bajc Cesnik, A., Darovic, S., Prpar Mihevc, S., Stalekar, M., Malnar, M., Motaln, H., Lee, Y.B., Mazej, J., Pohleven, J., Grosch, M., et al. (2019). Nuclear RNA foci from C9ORF72 expansion mutation form paraspeckle-like bodies. J. Cell Sci. *132*, jcs224303. https://doi.org/10.1242/jcs.224303.

59. Lee, Y.B., Chen, H.J., Peres, J.N., Gomez-Deza, J., Attig, J., Stalekar, M., Troakes, C., Nishimura, A.L., Scotter, E.L., Vance, C., et al. (2013). Hexanucleotide repeats in ALS/FTD form length-dependent RNA foci, sequester RNA binding proteins, and are neurotoxic. Cell Rep. *5*, 1178–1186. https://doi.org/10.1016/j.celrep.2013.10.049.

60. Gendron, T.F., Bieniek, K.F., Zhang, Y.J., Jansen-West, K., Ash, P.E.A., Caulfield, T., Daughrity, L., Dunmore, J.H., Castanedes-Casey, M., Chew, J., et al. (2013). Antisense transcripts of the expanded C9ORF72 hexanucleotide repeat form nuclear RNA foci and undergo repeat-associated non-ATG translation in c9FTD/ALS. Acta Neuropathol. *126*, 829–844. https://doi.org/10.1007/s00401-013-1192-8.

61. Mori, K., Weng, S.M., Arzberger, T., May, S., Rentzsch, K., Kremmer, E., Schmid, B., Kretzschmar, H.A., Cruts, M., Van Broeckhoven, C., et al. (2013). The C9orf72 GGGGCC repeat is translated into aggregating dipeptide-repeat proteins in FTLD/ALS. Science *339*, 1335–1338. https://doi.org/10.1126/science.1232927.

62. Kwon, I., Xiang, S., Kato, M., Wu, L., Theodoropoulos, P., Wang, T., Kim, J., Yun, J., Xie, Y., and McKnight, S.L. (2014). Poly-dipeptides encoded by the C9orf72 repeats bind nucleoli, impede RNA biogenesis, and kill cells. Science *345*, 1139–1145. https://doi.org/10.1126/science.1254917.

63. Boivin, M., Pfister, V., Gaucherot, A., Ruffenach, F., Negroni, L., Sellier, C., and Charlet-Berguerand, N. (2020). Reduced autophagy upon C9ORF72 loss synergizes with dipeptide repeat protein toxicity in G4C2 repeat expansion disorders. EMBO J. *39*, e100574. https://doi.org/10.15252/embj.2018100574.

64. Pal, A., Kretner, B., Abo-Rady, M., Glaβ, H., Dash, B.P., Naumann, M., Japtok, J., Kreiter, N., Dhingra, A., Heutink, P., et al. (2021). Concomitant gain and loss of function pathomechanisms in C9ORF72 amyotrophic lateral sclerosis. Life Sci. Alliance *4*, e202000764. https://doi.org/10.26508/lsa.202000764.

65. Didiot, M.C., Ferguson, C.M., Ly, S., Coles, A.H., Smith, A.O., Bicknell, A.A., Hall, L.M., Sapp, E., Echeverria, D., Pai, A.A., et al. (2018). Nuclear Localization of Huntingtin mRNA Is Specific to Cells of Neuronal Origin. Cell Rep. *24*, 2553–2560.e5. https://doi.org/10.1016/j.celrep.2018.07.106.

66. Jiang, H., Mankodi, A., Swanson, M.S., Moxley, R.T., and Thornton, C.A. (2004). Myotonic dystrophy type 1 is associated with nuclear foci of mutant RNA, sequestration of muscleblind proteins and deregulated alternative splicing in neurons. Hum. Mol. Genet. *13*, 3079–3088. https://doi.org/10.1093/hmg/ddh327.

67. Iwahashi, C.K., Yasui, D.H., An, H.J., Greco, C.M., Tassone, F., Nannen, K., Babineau, B., Lebrilla, C.B., Hagerman, R.J., and Hagerman, P.J. (2006). Protein composition of the intranuclear inclusions of FXTAS. Brain *129*, 256–271. https://doi.org/10.1093/brain/awh650.

68. Mankodi, A., Urbinati, C.R., Yuan, Q.P., Moxley, R.T., Sansone, V., Krym, M., Henderson, D., Schalling, M., Swanson, M.S., and Thornton, C.A. (2001). Muscleblind localizes to nuclear foci of aberrant RNA in myotonic dystrophy types 1 and 2. Hum. Mol. Genet. *10*, 2165–2170. https://doi.org/10.1093/hmg/10.19.2165.

69. Rudnicki, D.D., Holmes, S.E., Lin, M.W., Thornton, C.A., Ross, C.A., and Margolis, R.L. (2007). Huntington's disease–like 2 is associated with CUG repeat-containing RNA foci. Ann. Neurol. *61*, 272–282. https://doi.org/10.1002/ana.21081.

70. Zhou, B., Liu, C., Geng, Y., and Zhu, G. (2015). Topology of a G-quadruplex DNA formed by C9orf72 hexanucleotide repeats associated with ALS and FTD. Sci. Rep. *5*, 16673. https://doi.org/10.1038/srep16673.

71. Conlon, E.G., Lu, L., Sharma, A., Yamazaki, T., Tang, T., Shneider, N.A., and Manley, J.L. (2016). The C9ORF72 GGGGCC expansion forms RNA G-quadruplex inclusions and sequesters hnRNP H to disrupt splicing in ALS brains. Elife *5*, e17820. https://doi.org/10.7554/eLife.17820.

72. Khvorova, A., and Watts, J.K. (2017). The chemical evolution of oligonucleotide therapies of clinical utility. Nat. Biotechnol. *35*, 238–248. https://doi.org/10.1038/nbt.3765.

73. Hassler, M.R., Turanov, A.A., Alterman, J.F., Haraszti, R.A., Coles, A.H., Osborn, M.F., Echeverria, D., Nikan, M., Salomon, W.E., Roux, L., et al. (2018). Comparison of partially and fully chemically-modified siRNA in conjugate-mediated delivery in vivo. Nucleic Acids Res. *46*, 2185–2196. https://doi.org/10.1093/nar/gky037.

74. Ray, K.K., Wright, R.S., Kallend, D., Koenig, W., Leiter, L.A., Raal, F.J., Bisch, J.A., Richardson, T., Jaros, M., Wijngaard, P.L.J., et al. (2020). Two Phase 3 Trials of Inclisiran in Patients with Elevated LDL Cholesterol. N. Engl. J. Med. *382*, 1507–1519. https://doi.org/10.1056/NEJMoa1912387.

75. Brown, K.M., Nair, J.K., Janas, M.M., Anglero-Rodriguez, Y.I., Dang, L.T.H., Peng, H., Theile, C.S., Castellanos-Rizaldos, E., Brown, C., Foster, D., et al. (2022). Expanding RNAi therapeutics to extrahepatic tissues with lipophilic conjugates. Nat. Biotechnol. *40*, 1500–1508. https://doi.org/10.1038/s41587-022-01334-x.

76. Foster, D.J., Brown, C.R., Shaikh, S., Trapp, C., Schlegel, M.K., Qian, K., Sehgal, A., Rajeev, K.G., Jadhav, V., Manoharan, M., et al. (2018). Advanced siRNA Designs Further Improve In Vivo Performance of GalNAc-siRNA Conjugates. Mol. Ther. *26*, 708–717. https://doi.org/10.1016/j.ymthe.2017.12.021.

77. Davis, S.M., Hariharan, V.N., Lo, A., Turanov, A.A., Echeverria, D., Sousa, J., McHugh, N., Biscans, A., Alterman, J.F., Karumanchi, S.A., et al. (2022). Chemical optimization of siRNA for safe and efficient silencing of placental sFLT1. Mol. Ther. Nucleic Acids *29*, 135–149. https://doi.org/10.1016/j.omtn.2022.06.009.

78. Nair, J.K., Attarwala, H., Sehgal, A., Wang, Q., Aluri, K., Zhang, X., Gao, M., Liu, J., Indrakanti, R., Schofield, S., et al. (2017). Impact of enhanced metabolic stability on pharmacokinetics and pharmacodynamics of GalNAc-siRNA conjugates. Nucleic Acids Res. *45*, 10969–10977. https://doi.org/10.1093/nar/gkx818.

79. Ly, S., Navaroli, D.M., Didiot, M.C., Cardia, J., Pandarinathan, L., Alterman, J.F., Fogarty, K., Standley, C., Lifshitz, L.M., Bellve, K.D., et al. (2017). Visualization of self-delivering hydrophobically modified siRNA cellular internalization. Nucleic Acids Res. *45*, 15–25. https://doi.org/10.1093/nar/gkw1005.

80. Alterman, J.F., Coles, A.H., Hall, L.M., Aronin, N., Khvorova, A., and Didiot, M.C. (2017). A High-throughput Assay for mRNA Silencing in Primary Cortical Neurons in vitro with Oligonucleotide Therapeutics. Bio. Protoc. *7*, e2501. https://doi.org/10.21769/BioProtoc.2501.